

## Electronic Supporting Information for

# Highly electron deficient diketopyrrolopyrroles

By

Joshua Humphreys,<sup>a‡</sup> Ferdinando Malagrecia,<sup>a,b‡</sup> Paul A. Hume,<sup>c</sup> E. Stephen Davies,<sup>d</sup> Stephen P. Argent,<sup>d</sup> Tracey D. Bradshaw<sup>b</sup> and David B. Amabilino<sup>a,e\*</sup>.

<sup>a</sup> GSK Carbon Neutral Laboratories for Sustainable Chemistry, School of Chemistry, University of Nottingham, Triumph Road, Nottingham, NG7 2TU, UK

<sup>b</sup> School of Pharmacy, University of Nottingham, University Park, NG7 2RD, UK

<sup>c</sup> MacDiarmid Institute for Advanced Materials and Nanotechnology and School of Chemical and Physical Sciences, Victoria University of Wellington, Wellington 6010, New Zealand

<sup>d</sup> School of Chemistry, University of Nottingham, University Park, NG7 2RD, UK

<sup>e</sup> Institut de Ciència de Materials de Barcelona (ICMAB-CSIC), Consejo Superior de Investigaciones Científicas, Campus Universitari de Bellaterra, 08193 Cerdanyola del Vallès, Spain

<sup>‡</sup> These authors contributed equally to the work presented here.

## Materials and Methods

All commercially available reagents and solvents were used as received. The pyridyl DPP materials were prepared according to literature methods<sup>1</sup> with modifications, as noted below. Chromatography purifications were performed using Sigma-Aldrich Silica Gel (pore size 60Å, particle size 40-63 μm) and thin-layer chromatography (TLC) was carried out on E. Merck silica gel plates, irradiated using UV light (365 nm). NMR spectra were acquired on a Bruker AV400, Bruker AV(III)500, Jeol EX270 or Bruker DPX300 spectrometers and NMR spectra were recorded at room temperature, unless otherwise stated. All chemical shifts are reported in δ parts per million (ppm), using the solvent residual signal as an internal standard and the coupling constant values (*J*) are reported in Hertz (Hz). The following abbreviations are used for signal multiplicities: s, singlet; d, doublet; t, triplet; m, multiplet; and b, broad. Infra-red spectra were recorded on a Bruker Tensor 27 instrument equipped with a Pike GladiATR attachment with a diamond crystal. Melting points were determined on a Stuart SMP20 Melting Point Apparatus. Cyclic voltammetric studies were carried out using an Autolab PGSTAT20 potentiostat and in some cases an EmStat3 potentiostat. Standard cyclic voltammetry was carried out under an atmosphere of nitrogen using a three-electrode arrangement in a single compartment cell. A glassy carbon working electrode, a Pt wire secondary electrode and a saturated calomel reference electrode, chemically isolated from the test solution via a bridge tube containing electrolyte solution and fitted with a porous Vycor frit, were used in the cell when using the Autolab PGSTAT20 potentiostat. Redox potentials are quoted versus the ferrocenium-ferrocene couple, which was used as an internal reference. DMF was utilised as solvent. Tetrabutylammonium hexafluorophosphate was employed as supporting electrolyte for all electrochemical experiments.

UV/Vis absorption studies were performed using a Cary 5000 UV–Vis–NIR Absorption spectrometer. Emission studies were performed using an Edinburgh Instruments FLS980 Photoluminescence spectrometer. For quantum yield studies, for 4-**2**.2PF<sub>6</sub> and 4-**3**.2PF<sub>6</sub> fluorescence spectra were recorded as aerated solutions using a Jobin Yvon Horiba FluoroMax-3 spectrometer at ambient temperature in a 1 cm path length quartz cuvette. Quantum yields were calculated by comparison with the fluorescence observed for fluorescein (Φ = 0.91 in NaOH) under identical conditions of irradiation,<sup>2</sup> for 3-**2**.2PF<sub>6</sub> and 3-**3**.2PF<sub>6</sub> fluorescence spectra were recorded as aerated solutions using an Edinburgh Instruments FLS980 Photoluminescence spectrometer with Integrated sphere.

For spectroelectrochemical experiments the following concentrations were used 1.294 x 10<sup>-4</sup> moldm<sup>-3</sup> for 4-**2**.2PF<sub>6</sub>, 1.294 x 10<sup>-4</sup> moldm<sup>-3</sup> for 4-**3**.2PF<sub>6</sub>, 5.329 x 10<sup>-4</sup> moldm<sup>-3</sup> for 4-**2**.2PF<sub>6</sub> and 9.972 x 10<sup>-4</sup> moldm<sup>-3</sup> for 4-**3**.2PF<sub>6</sub>

HOMO and LUMO levels were calculated using the equations:

$$E_{\text{HOMO}} = - (E_{\text{onset}}(\text{ox}) + 4.8 \text{ [eV]}) \text{ and } E_{\text{LUMO}} = -(E_{\text{onset}}(\text{red}) + 4.8 \text{ [eV]}).$$

Band gap calculated from the onset of the optical absorption using the equation:

$$E_g = 1240 / \lambda_{\text{onset}} \text{ [eV]}.$$

Single crystals were selected and mounted using Fomblin® (YR-1800 perfluoropolyether oil) on a polymer-tipped MiTeGen MicroMount™ and cooled rapidly to 120 K in a stream of cold N<sub>2</sub> using an Oxford Cryosystems open flow cryostat.<sup>3</sup> 4-**2**.2PF<sub>6</sub> and 3-**3**.2PF<sub>6</sub> X-ray diffraction data were collected on an Oxford Diffraction SuperNova diffractometer (Atlas CCD area detector, mirror-monochromated Cu-Kα radiation source; λ = 1.54184 Å). X-ray diffraction measurements on crystals of 3-**2**.2PF<sub>6</sub> were performed in Experiments Hutch 1 (EH1) of Beamline I19, at Diamond Light Source.<sup>4</sup> The DLS data were collected at a wavelength of 0.6889 Å on a Fluid Film Devices 3-circle fixed-chi diffractometer using a Dectris Pilatus 2M detector. The crystal was mounted on a MiTeGen MicroMount™ using a perfluoropolyether oil and cooled for data collection by a Cryostream nitrogen-gas stream. The collected frames were integrated using XIA2

software<sup>5</sup> and the data were corrected for absorption effects using AIMLESS,<sup>6,7</sup> an empirical method. Cell parameters were refined from the observed positions of all strong reflections in each data set and absorption corrections were applied using a Gaussian numerical method with beam profile correction (CrysAlisPro).<sup>8</sup> The structures were solved within Olex2 by dual space iterative methods (SHELXT) and all non-hydrogen atoms refined by full-matrix least-squares on all unique F<sup>2</sup> values with anisotropic displacement parameters (SHELXL).<sup>9</sup> Hydrogen atoms were refined with constrained geometries and riding thermal parameters. Structures were checked with checkCIF.<sup>10</sup> CCDC-2160042-2160044 contains the supplementary data for these compounds. These data can be obtained free of charge from The Cambridge Crystallographic Data Centre via [www.ccdc.cam.ac.uk/data\\_request/cif](http://www.ccdc.cam.ac.uk/data_request/cif)

Special details for 4-2.2PF<sub>6</sub> Rigid bond and similarity restraints were applied to the anisotropic displacement parameters of the phosphorous and fluorine atoms of the hexafluorophosphate residues (SIMU, RIGU). The anisotropic displacement parameters of fluorine atoms F4 and F6 were restrained to have more isotropic character. These restraints on the hexafluorophosphate residues were likely necessary as a result of conformational disorder for which a sensible model could not be developed. The positions of the water and amide hydrogen atoms were located in the electron difference map and were refined with their O-H and N-H distances restrained to have target values of 0.84 and 0.88 Å respectively (DFIX, esd 0.02). The 1,3 intramolecular hydrogen distances of the water residues are restrained to target values of 1.32 Å (DFIX). The isotropic displacement parameters of the hydrogen atoms were constrained to be 1.5 times the U<sub>eq</sub> of their parent nitrogen and oxygen atoms. All other hydrogen atoms were geometrically placed and refined with a riding model.

Special details for 3-2.2PF<sub>6</sub> All hydrogen atoms were observed in the electron density map. The position of amide hydrogen H1 was refined with the N-H distance restrained to a target value of 0.88 Å (DFIX, esd 0.02 Å). All other hydrogen atoms were geometrically placed and refined with a riding model.

Special details for 3-3.2PF<sub>6</sub> pyrrolic lactone hydrogen H1 was refined and its N-H distance restrained to a target value of 0.88 Å (DFIX). The isotropic displacement parameter of H1 was constrained to have a value of 1.2 times U<sub>eq</sub> of its parent nitrogen atom N1. All other hydrogen atoms in the structure were observed in the electron density map before being geometrically placed and refined with a riding model.

## Theoretical calculations

Electronic structure calculations were performed using Gaussian 09.<sup>11</sup> All calculations used the B3LYP exchange-correlation functional equipped with the 6-311+G(d,p)<sup>12-14</sup> basis set with a ultrafine integration grid, and two-electron integral accuracy increased to 10<sup>-11</sup> PCM solvation with DMF as solvent.. Alkyl chains were replaced with ethyl groups to speed up the calculations. Energetic minima were confirmed by calculation and inspection of the vibrational modes, which showed zero imaginary frequencies in all cases. Optical gaps were calculated using linear response time dependent DFT at the geometry of the ground state. Solvent effects were treated with polarizable continuum model (integral equation formalism) with the default parameters for dimethylformamide.

## References

1. (a) T. He, Y. Gao, S. Sreejith, X. Tian, L. Liu, Y. Wang, H. Joshi, S. Z. F. Phua, S. Yao, X. Lin, Y. Zhao, A.C. Grimsdale, H. Sun, *Adv. Opt. Mater.* 2016, **4**, 746 (b) H. Ftouni, F. Bolze, J. Nicoud, *Dyes Pigm.* 2013, **97**, 77.
2. A. M. Brouwer, *Pure Appl. Chem.* 2011, **83**, 2213.
3. J. Cosier, A. M. Glazer, *J. Appl. Crystallogr.*, 1986, **19**, 105.
4. D. R. Allan, H. Nowell, S. A. Barnett, M. R. Warren, A. Wilcox, J. Christensen, L. K. Saunders, A. Peach, M. T. Hooper, L. Zaja, S. Patel, L. Cahill, R. Marshall, S. Trimnell, A. J. Foster, T. Bates, S. Lay, M. A. Williams, P. V. Hathaway, G. Winter, M. Gerstel R. W. Wooley, Source. *Crystals*, 2017, **7**, 336.
5. See <https://xia2.github.io/>
6. P. R. Evans, G. N. Murshudov, *Acta Cryst. D* 2013, **69**, 1204.
7. G. Winter, D. G. Waterman, J. M. Parkhurst, A. S. Brewster, R. J. Gildea, M. Gerstel, L. Fuentes-Montero, M. Vollmar, T. Michels-Clark, I. D. Young, N. K. Sauter G. Evans, *Acta Crystallogr. Sect. D-Struct. Biol.*, 2018, **74**, 85.
8. Rigaku Oxford Diffraction, (2018), CrysAlisPro Software system, version 1.171.40.45a, Rigaku Corporation, Oxford, UK.
9. V. Dolomanov, L. J. Bourhis, R. J. Gildea, J. A. K. Howard, H. Puschmann, *J. Appl. Cryst.* 2009, **42**, 339.
10. See <http://checkcif.iucr.org/> last accessed on 20/8/2022.
11. Gaussian 09, Revision D.01, M. J. Frisch, G. W. Trucks, H. B. Schlegel, G. E. Scuseria, M. A. Robb, J. R. Cheeseman, G. Scalmani, V. Barone, B. Mennucci, G. A. Petersson, H. Nakatsuji, M. Caricato, X. Li, H. P. Hratchian, A. F. Izmaylov, J. Bloino, G. Zheng, J. L. Sonnenberg, M. Hada, M. Ehara, K. Toyota, R. Fukuda, J. Hasegawa, M. Ishida, T. Nakajima, Y. Honda, O. Kitao, H. Nakai, T. Vreven, J. A. Montgomery, Jr., J. E. Peralta, F. Ogliaro, M. Bearpark, J. J. Heyd, E. Brothers, K. N. Kudin, V. N. Staroverov, T. Keith, R. Kobayashi, J. Normand, K. Raghavachari, A. Rendell, J. C. Burant, S. S. Iyengar, J. Tomasi, M. Cossi, N. Rega, J. M. Millam, M. Klene, J. E. Knox, J. B. Cross, V. Bakken, C. Adamo, J. Jaramillo, R. Gomperts, R. E. Stratmann, O. Yazyev, A. J. Austin, R. Cammi, C. Pomelli, J. W. Ochterski, R. L. Martin, K. Morokuma, V. G. Zakrzewski, G. A. Voth, P. Salvador, J. J. Dannenberg, S. Dapprich, A. D. Daniels, O. Farkas, J. B. Foresman, J. V. Ortiz, J. Cioslowski, and D. J. Fox, Gaussian, Inc., Wallingford CT, 2013.
12. A. D. Becke, *Phys. Rev. A* 1988, **38**, 3098.
13. A. D. Becke, *J. Chem. Phys.* 1993, **98**, 5648.
14. C. Lee, W Yang, R. G. Parr, *Phys. Rev. B* 1988, **37**, 785.

**Table S1.** Crystallographic experimental details.

	4-2.2PF <sub>6</sub>	3-2.2PF <sub>6</sub>	3-3.2PF <sub>6</sub>
Chemical formula	2(F <sub>6</sub> P)·C <sub>28</sub> H <sub>36</sub> N <sub>4</sub> O <sub>2</sub> ·2(H <sub>2</sub> O)	C <sub>28</sub> H <sub>36</sub> N <sub>4</sub> O <sub>2</sub> ·2(F <sub>6</sub> P)	C <sub>30</sub> H <sub>24</sub> N <sub>4</sub> O <sub>2</sub> ·2(C <sub>2</sub> H <sub>3</sub> N)·2(F <sub>6</sub> P)
<i>M<sub>r</sub></i>	786.58	750.55	844.58
Crystal system, space group	Triclinic, <i>P</i> -1	Monoclinic, <i>C2/c</i>	Monoclinic, <i>P2<sub>1</sub>/n</i>
Temperature (K)	120	100	120
<i>a</i> , <i>b</i> , <i>c</i> (Å)	9.2788 (8), 9.8717 (7), 19.406 (2)	34.9289 (7), 9.64811 (19), 9.32463 (17)	6.56026 (5), 13.16435 (8), 21.40535 (13)
$\alpha$ , $\beta$ , $\gamma$ (°)	94.465 (7), 99.481 (8), 97.531 (6)	90, 96.9621 (18), 90	90, 95.7893 (6), 90
<i>V</i> (Å <sup>3</sup> )	1729.1 (3)	3119.21 (7)	1839.17 (2)
<i>Z</i>	2	4	2
Radiation type	Cu <i>K</i> $\alpha$	Synchrotron, $\lambda$ = 0.6889 Å	Cu <i>K</i> $\alpha$
$\mu$ (mm <sup>-1</sup> )	2.10	0.23	2.01
Crystal size (mm)	0.19 × 0.11 × 0.02	0.08 × 0.03 × 0.01	0.37 × 0.06 × 0.04
Diffractometer	SuperNova, Dual, Cu at zero, Atlas	Fluid Film Devices, Dectris Pilatus 2M	XtalLAB PRO <i>MM007</i> , PILATUS3 R 200K
<i>T<sub>min</sub></i> , <i>T<sub>max</sub></i>	0.953, 0.993	0.994, 1.0	0.620, 1.000
No. of measured, independent and observed [ <i>I</i> > 2 $\sigma$ ( <i>I</i> )] reflections	16104, 6212, 3507	24129, 4749, 3386	40002, 3779, 3581
<i>R<sub>int</sub></i>	0.099	0.067	0.039
( <i>sin</i> $\theta$ / $\lambda$ ) <sub>max</sub> (Å <sup>-1</sup> )	0.599	0.714	0.627
<i>R</i> [ <i>F</i> <sup>2</sup> > 2 $\sigma$ ( <i>F</i> <sup>2</sup> )], <i>wR</i> ( <i>F</i> <sup>2</sup> ), <i>S</i>	0.087, 0.259, 1.02	0.046, 0.117, 1.09	0.043, 0.116, 1.07
No. of reflections	6212	4749	3779
No. of parameters	471	221	257
No. of restraints	361	175	1
$\Delta\rho$ <sub>max</sub> , $\Delta\rho$ <sub>min</sub> (e Å <sup>-3</sup> )	1.08, -0.56	0.57, -0.52	0.86, -0.46
CDCC	2160042	2160043	2160044

H atoms were treated by a mixture of independent and constrained refinement.

**3,6-Di(pyridin-4-yl)-2,5-dihydropyrrolo[3,4-c]pyrrole-1,4-dione (4-1)** : Sodium (4.51 g, 196 mmol) and a catalytic amount of iron chloride were added to anhydrous *t*-amyl alcohol (50 ml, 46 mmol) and heated at 120 °C for 1 hour, under an argon atmosphere, whilst stirring, until all the sodium had dissolved. The mixture was then cooled to around 80 °C and 4-pyridinecarbonitrile (5.01 g, 4.81 mmol) added. The reaction was then heated slowly to 130 °C and once it had reached this temperature diethyl succinate (5.0 ml, 3.0 mmol) in *t*-amyl alcohol (15 ml, 140 mmol) was added *via* syringe pump over 3 hours. Once added, the reaction was allowed to heat at 130 °C overnight. Upon completion, the reaction mixture was cooled to 50 °C and glacial acetic acid (50 ml, 1.2 mol) added and the solution refluxed at 118 °C for 1 hour. The mixture was then filtered, washed with hot methanol and allowed to dry in a vacuum desiccator to afford the pure product as a red solid (6.95 g, 2.39 mmol, 50 %).  $\nu_{\text{max}}$  (FT-ATR-IR) 3123 (NH stretch), 1648 (C=O), 1588 (C=C stretch), 1543, 1504, 1442, 1368, 1294, 1232, 1197, 1143, 1081, 1038, 1014, 896, 818, 744, 663, 628, 461, 424  $\text{cm}^{-1}$ .

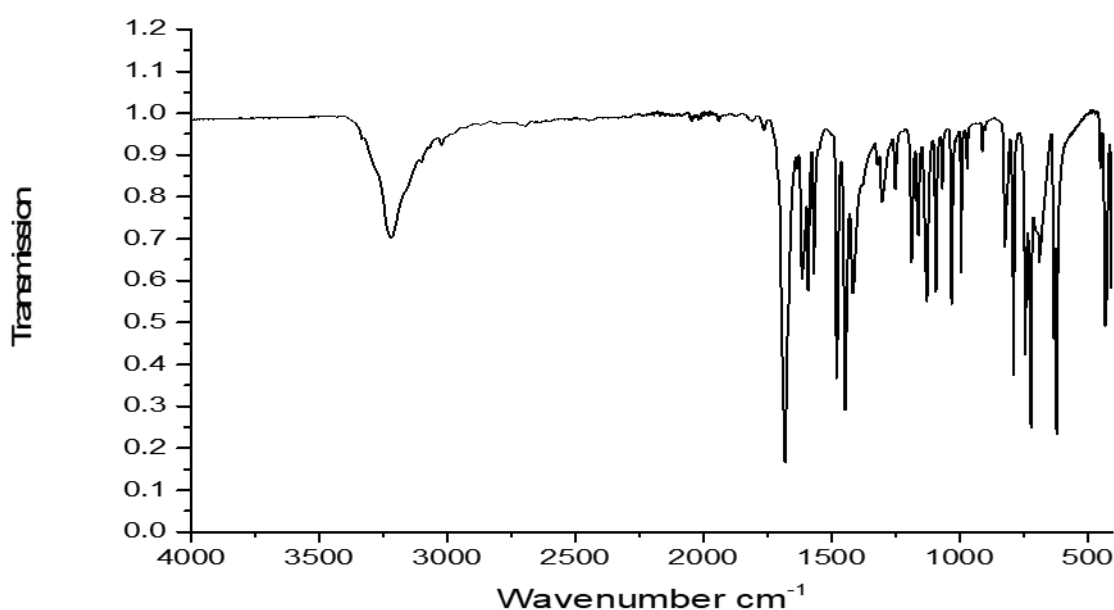
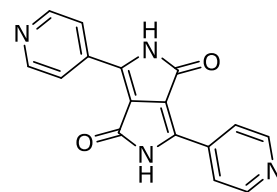
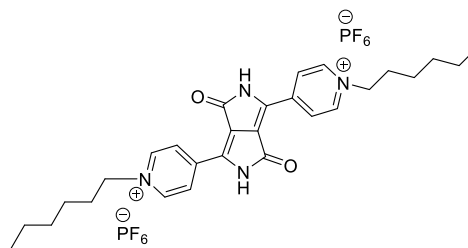


**Figure S1.** FT-IR of 4-1

**4,4'-(3,6-Dioxo-2,3,5,6-tetrahydropyrrolo[3,4-c]pyrrole-1,4-diyl)bis(1-hexylpyridin-1-ium)3,6-Di(pyridin-4-yl)-2,5 (4-2.2PF<sub>6</sub>) bis(hexafluorophosphate):**

3,6-Di(pyridin-4-yl)-2,5-dihydropyrrolo[3,4-c]pyrrole-1,4-dione (**4-1**) (0.20 g, 69  $\mu$ mol) was added to hexyl iodide (20 ml, 0.14 mol) and heated at 150 °C for several days, under argon atmosphere whilst stirring. Upon completion, the reaction mixture was cooled and then filtered, washed with hexane DCM and allowed to dry to give the crude product, which was purified by column chromatography using an eluent system of 95:5 acetonitrile: KPF<sub>6</sub>



(aq.) followed by washing with water and refiltering to get rid of excess salt to yield the product a dark purple solid (85 mg, 19  $\mu$ mol, 27%). m.p. 225-228 °C;  $\nu_{\text{max}}$  (FT-ATR-IR) 3143 (NH stretch), 3077 (CH stretch), 3014 (CH stretch), 2929 (CH stretch), 2861 (CH stretch), 1662(C=O), 1563 (C=C stretch), 1520, 1469, 1434, 1380, 1310, 1234, 1172, 1135, 1038, 828, 748, 622, 556, 449  $\text{cm}^{-1}$ ; <sup>1</sup>H NMR (300 MHz, CD<sub>3</sub>CN)  $\delta$  9.67 (2 H, bs, NH), 8.83 (4 H, d, *J* 6.3 Hz, ArH), 8.74 (4 H, d, *J* 5.6 Hz, ArH), 4.55 (4 H, t, *J* 7.3 Hz, N-CH<sub>2</sub>), 1.50-1.26 (16 H, m, RCH<sub>2</sub>), 0.90 (6 H, t, *J* 6.8 Hz, R-CH<sub>3</sub>) ppm; <sup>13</sup>C NMR (100 MHz, CD<sub>3</sub>CN)  $\delta$  162.0, 146.3, 142.4, 141.6, 126.4, 63.0, 55.3, 31.7, 31.7, 26.2, 23.0, 14.2 ppm. Elemental analysis calculated for C<sub>28</sub>H<sub>36</sub>N<sub>4</sub>O<sub>2</sub>P<sub>2</sub>F<sub>12</sub>: C, 44.81; H, 4.83; N, 7.46%; found C, 44.59 H, 4.45; N, 7.25%. MALDI-TOF-MS found [M-2PF<sub>6</sub>]<sup>+</sup> 460.402 required for C<sub>28</sub>H<sub>36</sub>N<sub>4</sub>O<sub>2</sub><sup>2+</sup> 460.283.

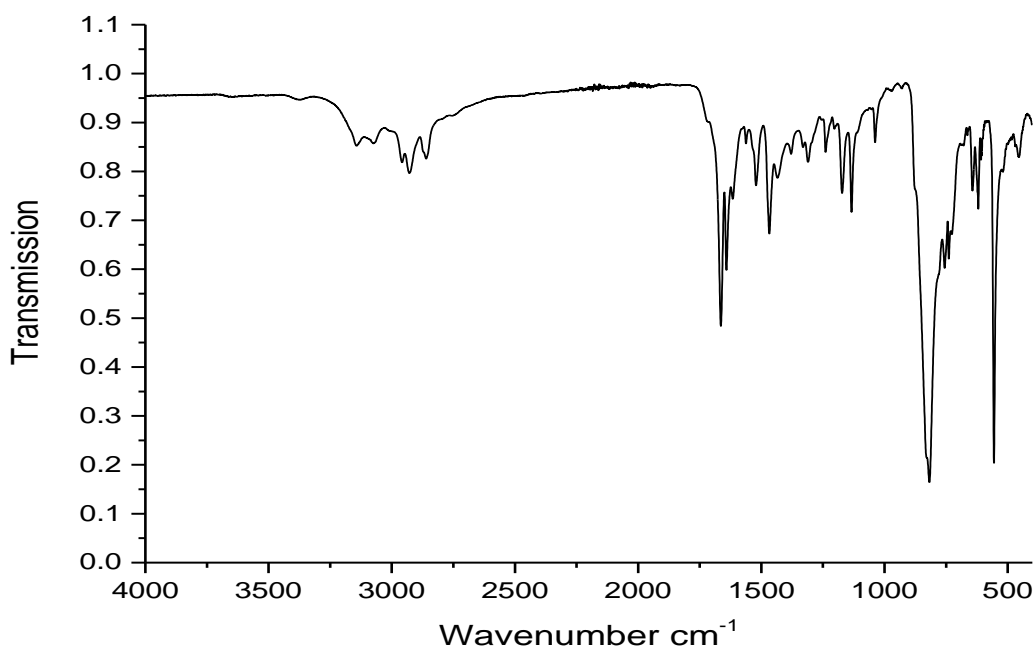


**Figure S2.** FT-IR of 4-2.2PF<sub>6</sub>.

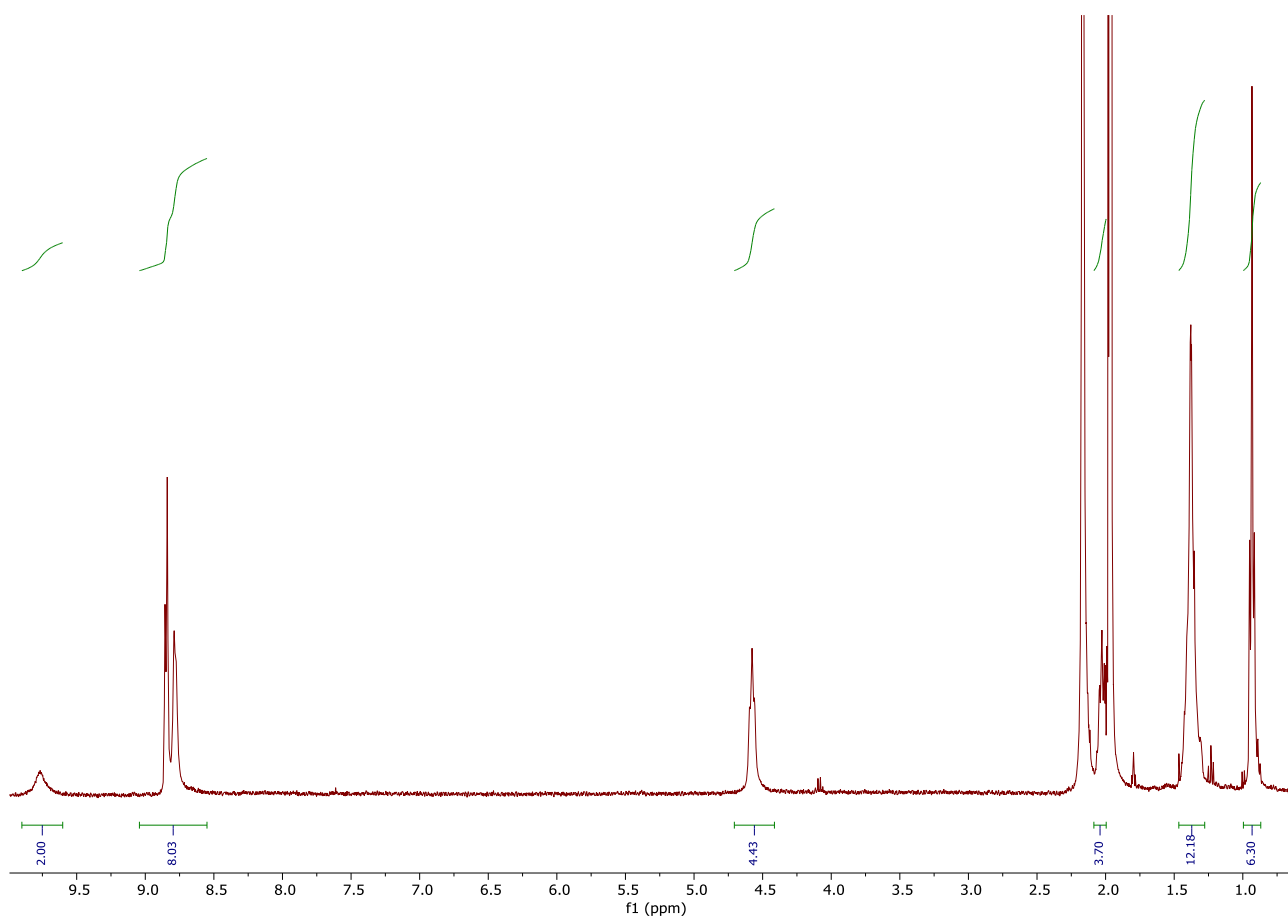


Figure S3.  $^1\text{H}$  NMR of 4-2.2PF<sub>6</sub> recorded in acetonitrile d<sub>3</sub>.

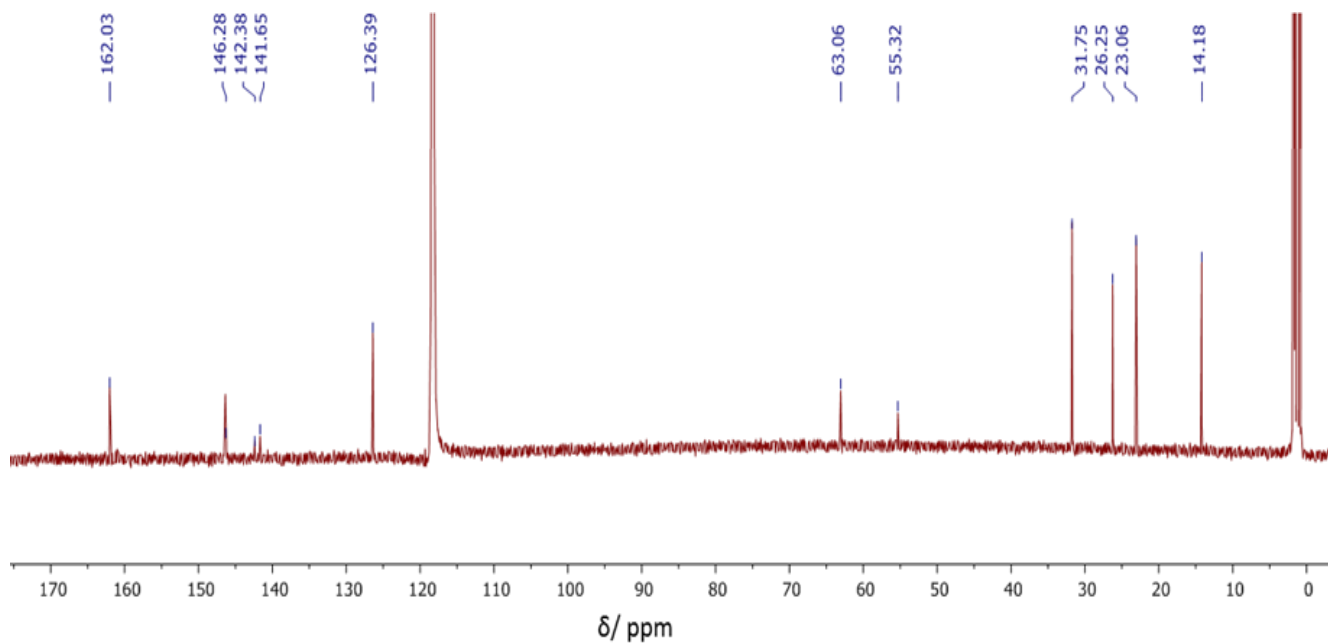
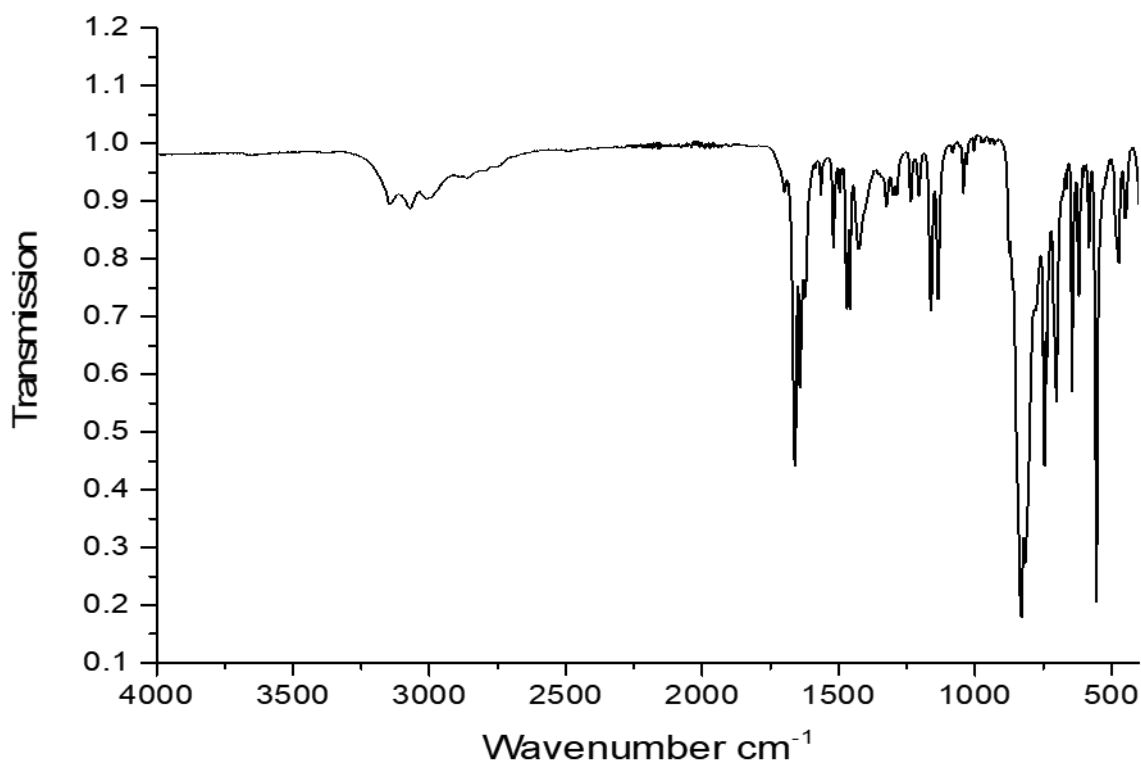
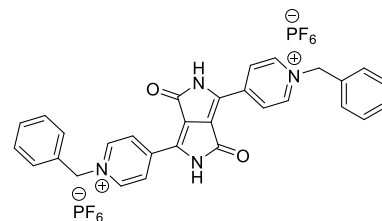


Figure S4.  $^{13}\text{C}$  NMR of 4-2.2PF<sub>6</sub> recorded in acetonitrile d<sub>3</sub>.

**4,4'-(3,6-Dioxo-2,3,5,6-tetrahydropyrrolo[3,4-c]pyrrole-1,4-diyl)bis(1-benzylpyridin-1-ium) bis(hexafluorophosphate) (4-3.2PF<sub>6</sub>):**

3,6-Di(pyridin-4-yl)-2,5-dihydropyrrolo[3,4-c]pyrrole-1,4-dione (**4-1**) (250mg, 86.2 μmol) was added to benzyl chloride (20 ml, 170 mmol) and heated at 150 °C for five days, under an argon atmosphere whilst stirring. The cooled reaction mixture was filtered, washed with hexane and DCM and allowed to dry to give the crude product, which was purified by column chromatography using an eluent system of 95:5 acetonitrile: KPF<sub>6</sub> (aq.) followed by washing with water and re-filtering to get rid of excess salt to yield the product a purple solid (158 mg, 33.5 μmol, 39%). m.p. 228–232 °C;  $\nu_{\max}$  (FT-ATR-IR) 3141(NH stretch), 3073 (CH stretch), 3007(CH stretch), 2855(CH stretch), 1660 (C=O), 1566 (C=C stretch), 1518, 1469, 1425, 1325, 1236, 1205, 1162, 1135, 1042, 832, 746, 702, 645, 556, 474 cm<sup>-1</sup>; <sup>1</sup>H NMR  $\delta_{\text{H}}$  (300 MHz, CD<sub>3</sub>CN) 9.81 (2 H, bs, NH), 8.90 (4 H, d, *J* 7.0 Hz, ArH), 8.72 (4 H, d, *J* 7.0 Hz, ArH), 7.52–7.48 (10 H, m, ArH), 5.75 (4 H, m, CH<sub>2</sub>) ppm; <sup>13</sup>C NMR  $\delta_{\text{C}}$  (100 MHz, CD<sub>3</sub>CN) 161.9, 146.4, 142.3, 142.0, 133.5, 131.0, 130.6, 130.4, 126.5, 65.6 ppm. Elemental analysis calculated for C<sub>30</sub>H<sub>24</sub>N<sub>4</sub>O<sub>2</sub>P<sub>2</sub>F<sub>12</sub>: C, 47.26; H, 3.17; N, 7.35%; found C, 47.45 H, 2.95; N, 6.50 %. MALDI-TOF-MS found [M-2PF<sub>6</sub>]<sup>+</sup> 472.307 required for C<sub>30</sub>H<sub>24</sub>N<sub>4</sub>O<sub>2</sub> 472.189.



**Figure S5.** FT-ATR-IR of 4-3.2PF<sub>6</sub>

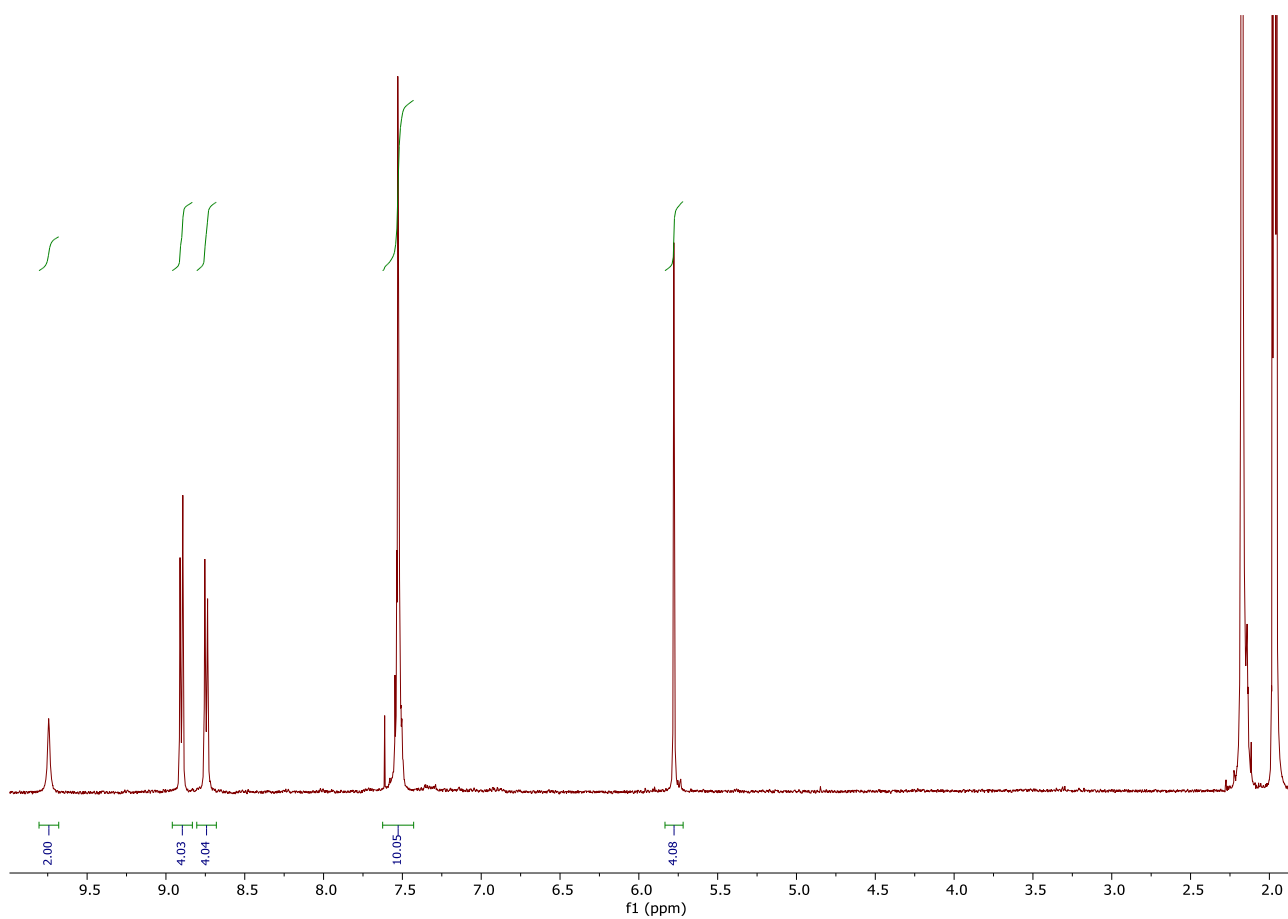


Figure S6.  $^1\text{H}$  NMR of 4-3.2PF<sub>6</sub> recorded in acetonitrile d<sub>3</sub>.

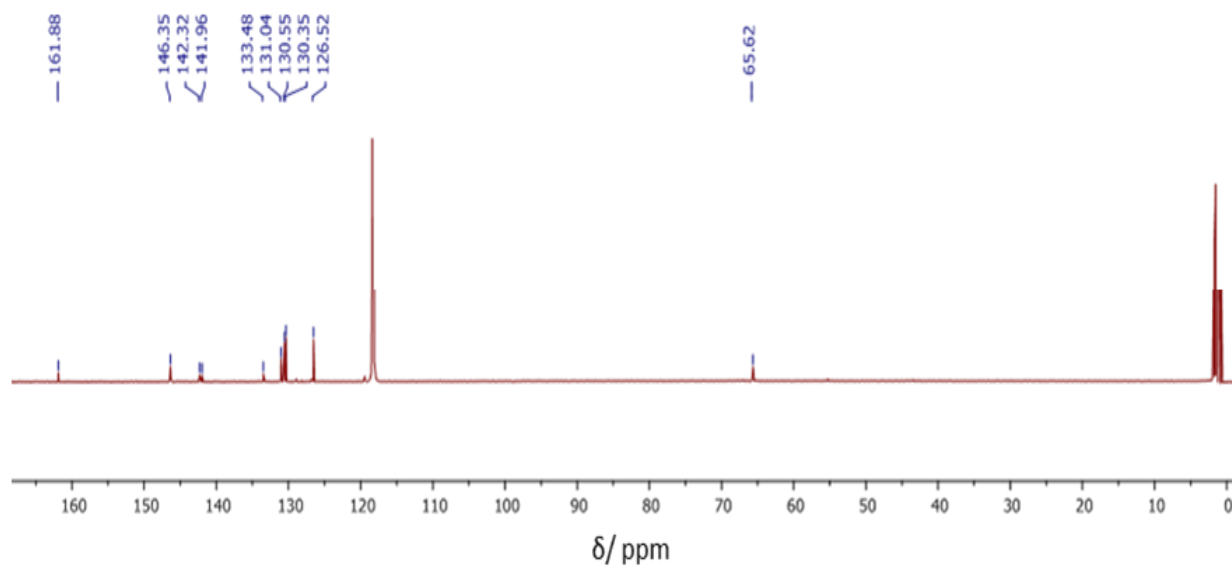


Figure S7.  $^{13}\text{C}$  NMR of 4-3.2PF<sub>6</sub> recorded in acetonitrile d<sub>3</sub>.

### 3,6-Di(pyridin-3-yl)-2,5-dihydropyrrolo[3,4-c]pyrrole-1,4-dione (3-1):

Sodium (4.51 g, 196 mmol) and a catalytic amount of iron chloride were added to anhydrous *t*-amyl alcohol (50 ml, 460 mmol) and heated at 120 °C for 1 hour, under an argon atmosphere, whilst stirring, until all the sodium had dissolved. The mixture was then cooled to 90 °C and 4-pyridinecarbonitrile (5.01 g, 4.81 mmol) added. The reaction was then heated slowly to 130 °C and once it had reached this temperature diethyl succinate (5.0 ml, 3.0 mmol) in *t*-amyl alcohol (15 ml, 0.14 mol) was added via syringe pump over 3 hours. Once added, the reaction was allowed to heat at 130 °C overnight. Upon completion, the reaction mixture was cooled to 50 °C and glacial acetic acid (50 ml, 1.2 mol) added slowly and the solution refluxed at 118 °C for 1 hour. The mixture was then filtered over a glass sintered crucible, washed with hot methanol and allowed to dry in a vacuum desiccator to afford the pure product as a dark red solid (10.43 g, 3.59 mmol, 75 %).  $\nu_{\max}$  (FT-ATR-IR) 3207 (NH stretch), 1684 (C=O), 1588 (C=C stretch), 1567, 1481, 1439, 1407, 1293, 1245, 1193, 1123, 1085, 1032, 989, 816, 789, 716, 676, 620, 423  $\text{cm}^{-1}$ .

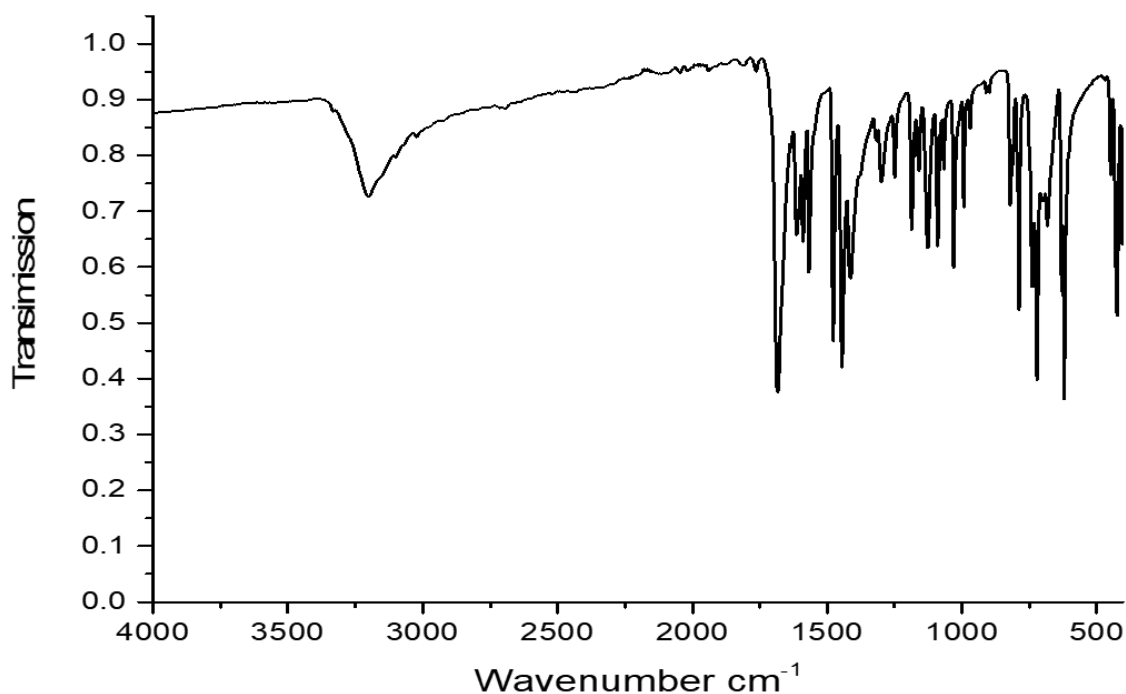
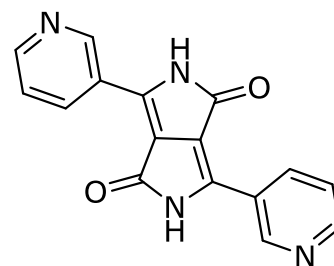
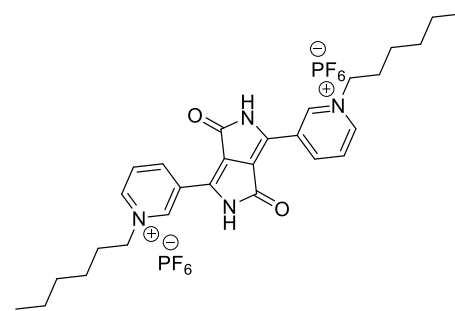


Figure S8. FT-ATR-IR of 3-1.

**3,3'-(3,6-Dioxo-2,3,5,6-tetrahydropyrrolo[3,4-c]pyrrole-1,4-**

**diyl)bis(1- hexylpyridin-1-ium) (3-2.2PF<sub>6</sub>):** 3,6-Di(pyridin-3-yl)-2,5-dihydropyrrolo[3,4-c]pyrrole-1,4-dione (500 mg, 1.74 mmol) was added to hexyl iodide (10 ml, 84 mmol) and heated at 150 °C for five days, under an argon atmosphere whilst stirring. Upon completion, the reaction mixture was cooled and then filtered over a glass sintered crucible and washed with methanol and acetonitrile and allowed to dry give the compound as orange solid, then the solid was dissolved in hot water (500mL) followed



by addition of K<sub>2</sub>PF<sub>6</sub> (400 mg), the resulting bright orange solid was then filtered and washed with water (2 × 50 mL) (170mg, 38 μmol, 54%). m.p. 226–228 °C;  $\nu_{\max}$  (FT-ATR-IR) 3395 (NH stretch), 3085 (CH stretch), 3014 (CH stretch), 2925 (CH stretch), 2858 (CH stretch), 1687(C=O), 1641 (N-H bending), 1602, 1517 (C=C stretch), 1460, 1427, 1311, 1217, 1188, 1143, 1107, 1058, 1024, 827, 734, 677, 599, 555, 505 cm<sup>-1</sup>; <sup>1</sup>HNMR  $\delta_{\text{H}}$  (400 MHz, d<sub>6</sub> DMSO) 11.99 (2H, s, N-H), 9.82 (2H, s, Ar-H), 9.35–9.33 (2H, d, *J* 8.3 Hz, Ar-H), 9.26–9.25 (2H, d, *J* 6.1 Hz, Ar-H), 8.46–8.43 (2H, m, *J* 8.3 Hz, ArH), 4.71–4.67 (4H, t, *J* 7.5Hz, N<sup>+</sup>-CH<sub>2</sub>), 2.09–2.02 (4H, q, *J* 7.39 Hz, N<sup>+</sup>-CH<sub>2</sub>-CH<sub>2</sub>), 1.38–1.28 (12H, m), 0.90–0.87 (6H, t, *J* 7.29 Hz, -CH<sub>3</sub>); <sup>13</sup>C NMR  $\delta_{\text{C}}$  (75 MHz, d<sub>6</sub> DMSO) 162.2, 146.7, 143.9, 142.4, 129.1, 127.7, 114.1, 62.3, 31.0, 30.4, 25.4, 22.2, 14.3; MALDI-TOF-MS found [M-2PF<sub>6</sub>]<sup>+</sup> 460.402 required for C<sub>28</sub>H<sub>36</sub>N<sub>4</sub>O<sub>2</sub><sup>2+</sup> 460.283.

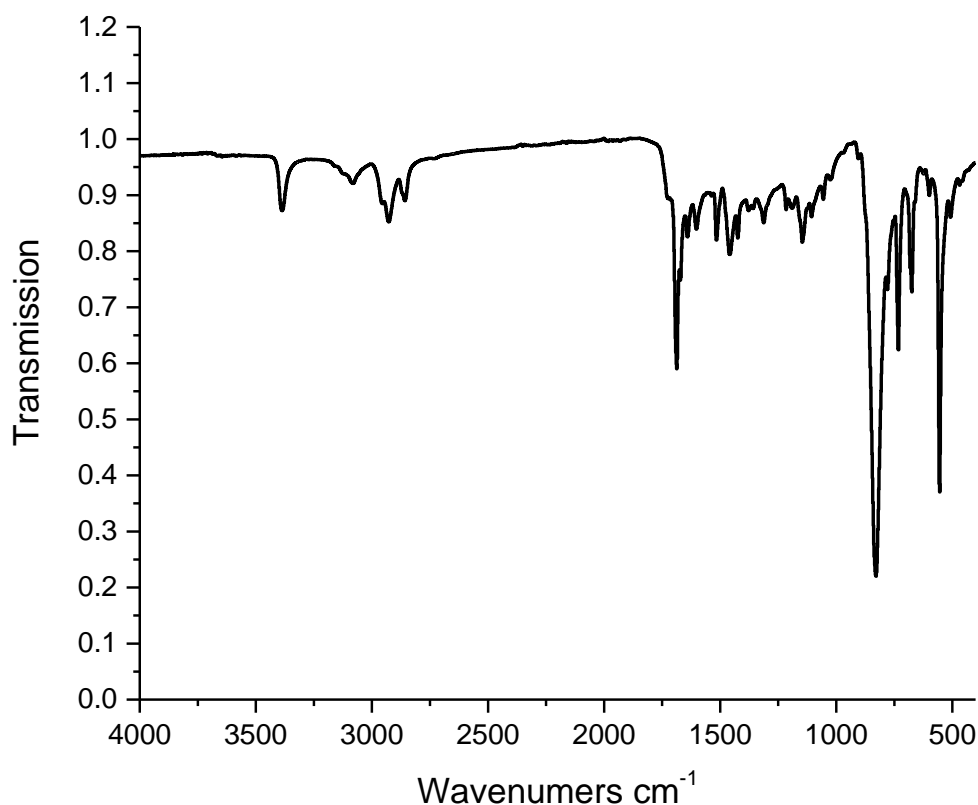


**Figure S9.** FT-ATR-IR of 3-2.2PF<sub>6</sub>.

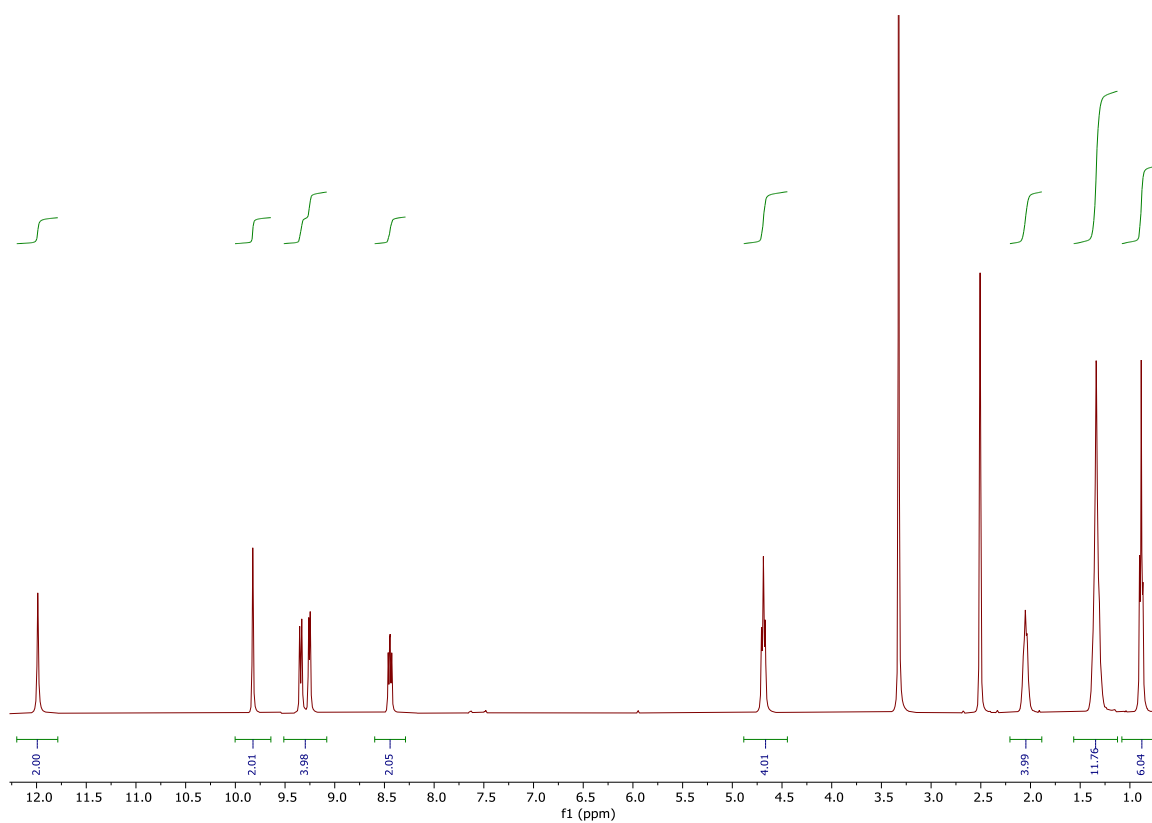


Figure S10.  $^1\text{H}$  NMR of 3-2.2PF<sub>6</sub> recorded in DMSO d<sub>6</sub>.

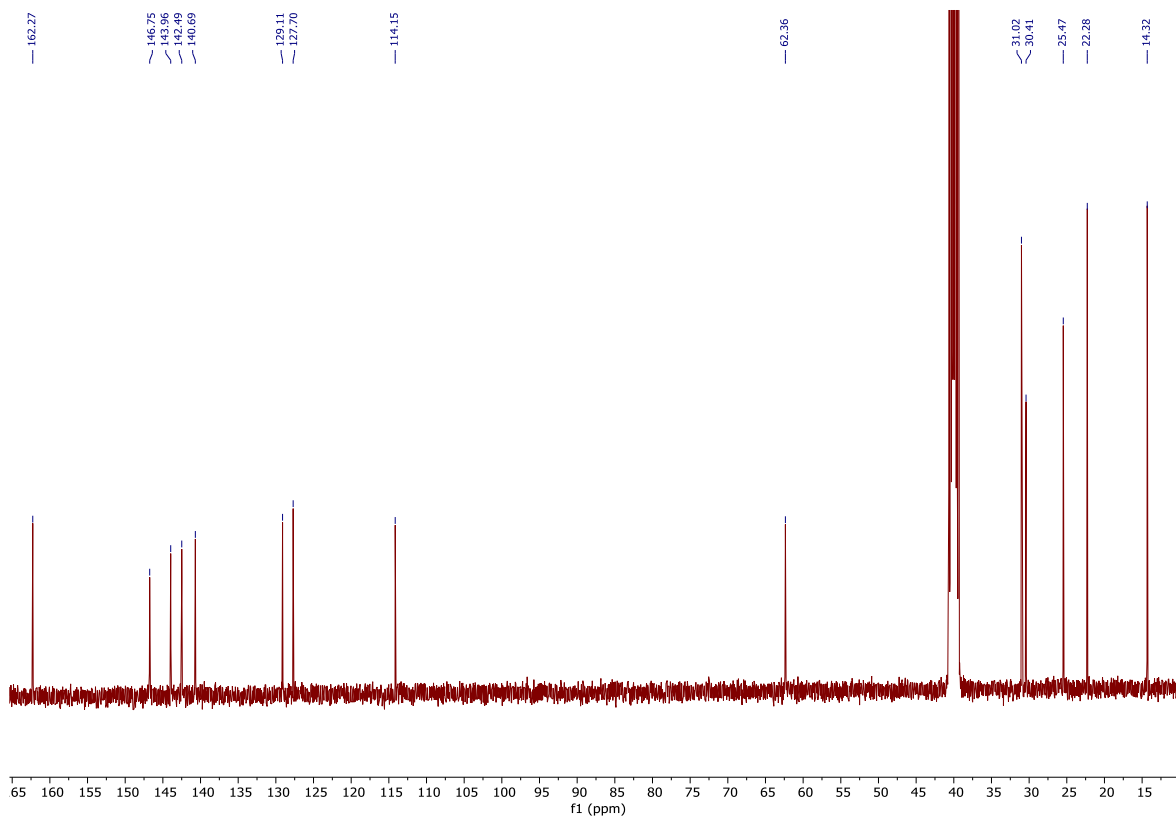
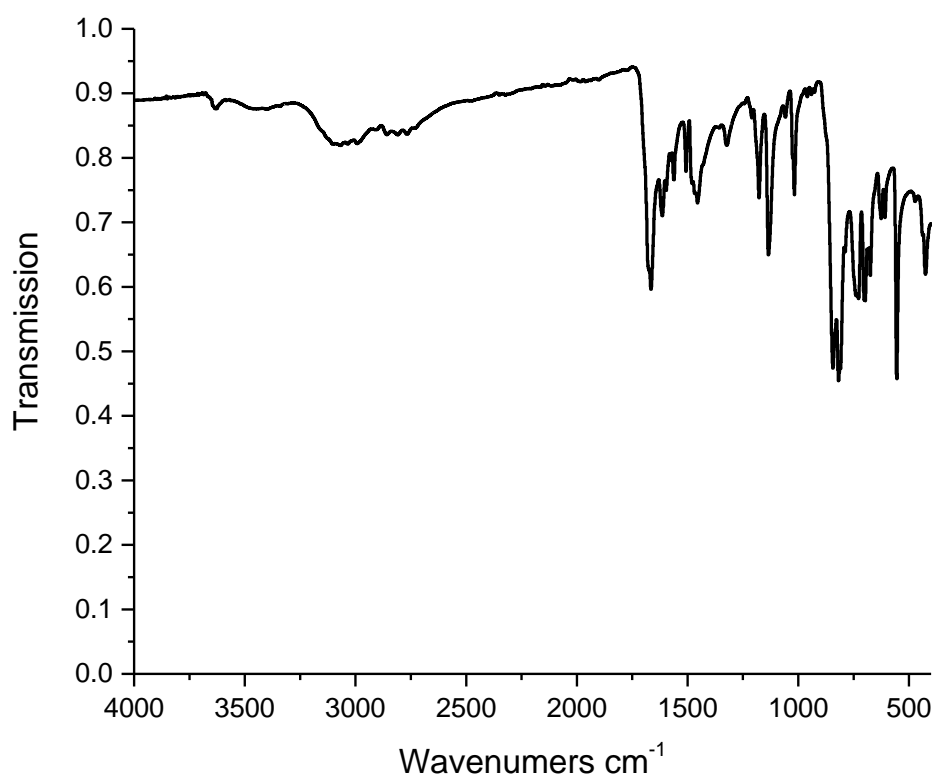
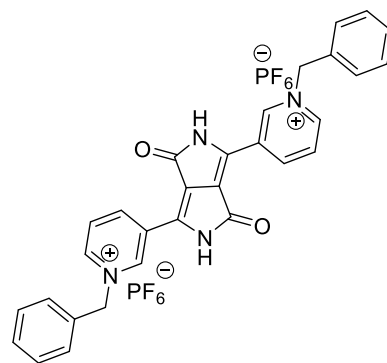


Figure S11.  $^{13}\text{C}$  NMR of 3-2.2PF<sub>6</sub> recorded in DMSO d<sub>6</sub>.

**3,3'-(3,6-Dioxo-2,3,5,6-tetrahydropyrrolo[3,4-c]pyrrole-1,4-diyl)bis(1-benzylpyridin-1-ium) bis(hexafluorophosphate) (3-3.2PF<sub>6</sub>):** 3,6-Di(pyridin-3-yl)-2,5-dihydropyrrolo[3,4-c]pyrrole-1,4-dione (1.0 g, 3.48 mmol) was added to benzyl bromide (10 ml, 84 mmol) and heated at 150 °C for five days, under argon atmosphere whilst stirring. The cooled reaction mixture was filtered over a glass sintered crucible and washed with dichloromethane and acetonitrile and allowed to dry to give the compound as orange solid, then the solid was dissolved in hot water (500mL) followed by addition of KPF<sub>6</sub> (400 mg), the resulting bright orange solid was then filtered and washed with water (2 × 50 mL) (1.458 g, 1.91 mmol, 54%). m.p. 229–233 °C;  $\nu_{\max}$  (FT-ATR-IR) 3627, 3430 (NH stretch), 3064 (CH stretch), 3037 (CH stretch), 2991 (CH stretch), 2861 (CH stretch), 2811 (CH stretch), 1664(C=O), 1614(N-H bending) 1562 (C=C stretch), 1508, 1454, 1322, 1211, 1178, 1135, 1058, 1018, 958, 929, 817, 727, 701, 676, 628, 609, 555, 474, 449 cm<sup>-1</sup>; <sup>1</sup>H NMR  $\delta_{\text{H}}$  (300 MHz, CD<sub>3</sub>CN) 9.96 (2H, s ArH), 9.68 (2H, s, NH) 9.00–8.98 (2H, d, *J* 8.5 Hz, ArH) 8.90–8.88 (2H, d, *J* 6.1 Hz, ArH) 8.27–8.23 (2H, m, *J* 7.1 Hz, ArH) 7.60–7.53(10H, m, ArH) 5.84(4H, s, CH); <sup>13</sup>C NMR  $\delta_{\text{C}}$  (75 MHz, CD<sub>3</sub>CN) 162.2, 146.6, 145.2, 143.0, 140.5, 133.1, 131.1 130.6, 130.2, 129.2, 115.3, 66.7; MALDI-TOF-MS found [M-2PF<sub>6</sub>]<sup>+</sup> 472.245 required for C<sub>30</sub>H<sub>24</sub>N<sub>4</sub>O<sub>2</sub> 472.189.



**Figure S12.** FT-IR of 3-3.2PF<sub>6</sub>.

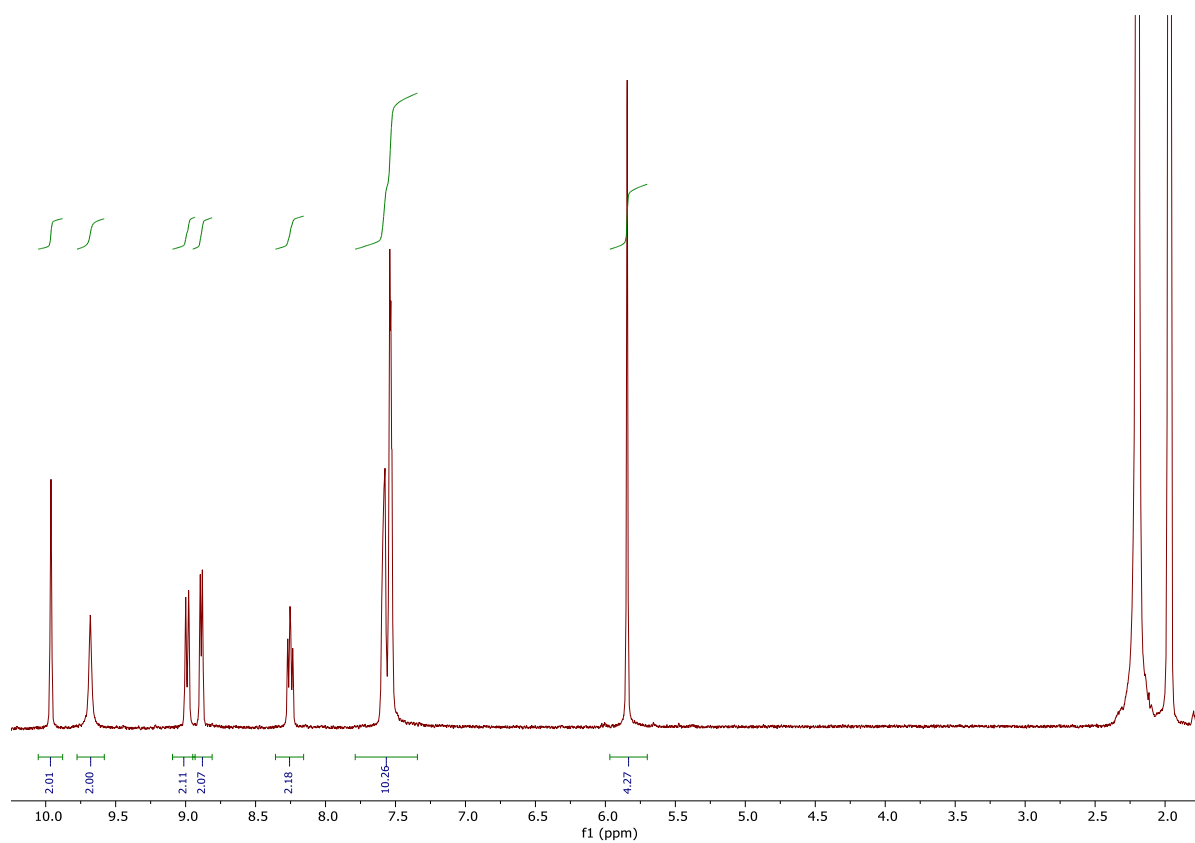


Figure S13.  $^1\text{H}$  NMR of 3-3.2PF<sub>6</sub> recorded in acetonitrile d<sub>3</sub>.

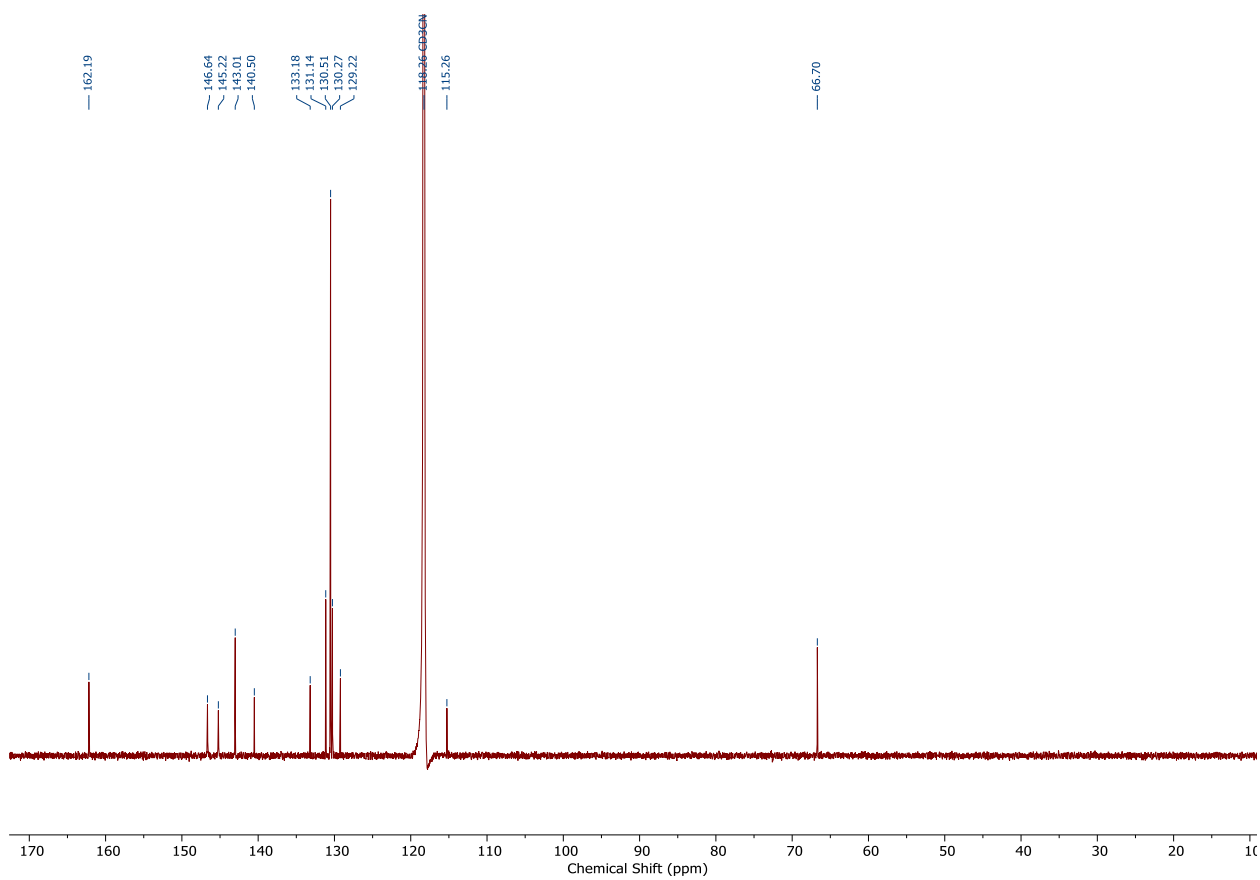
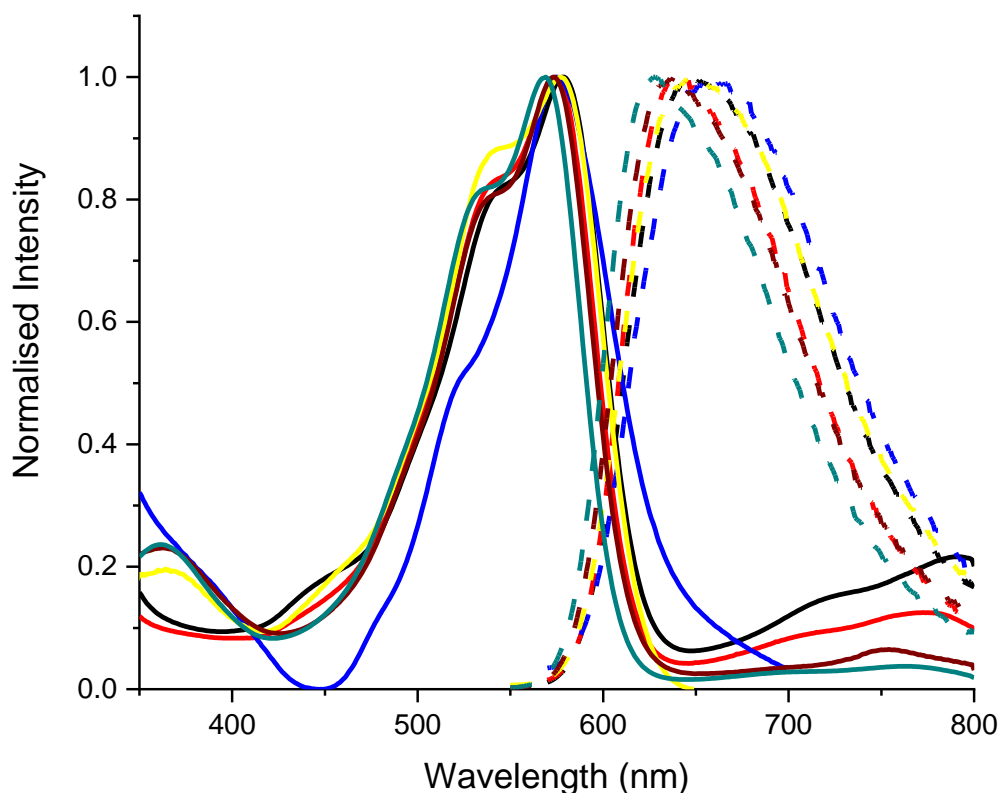


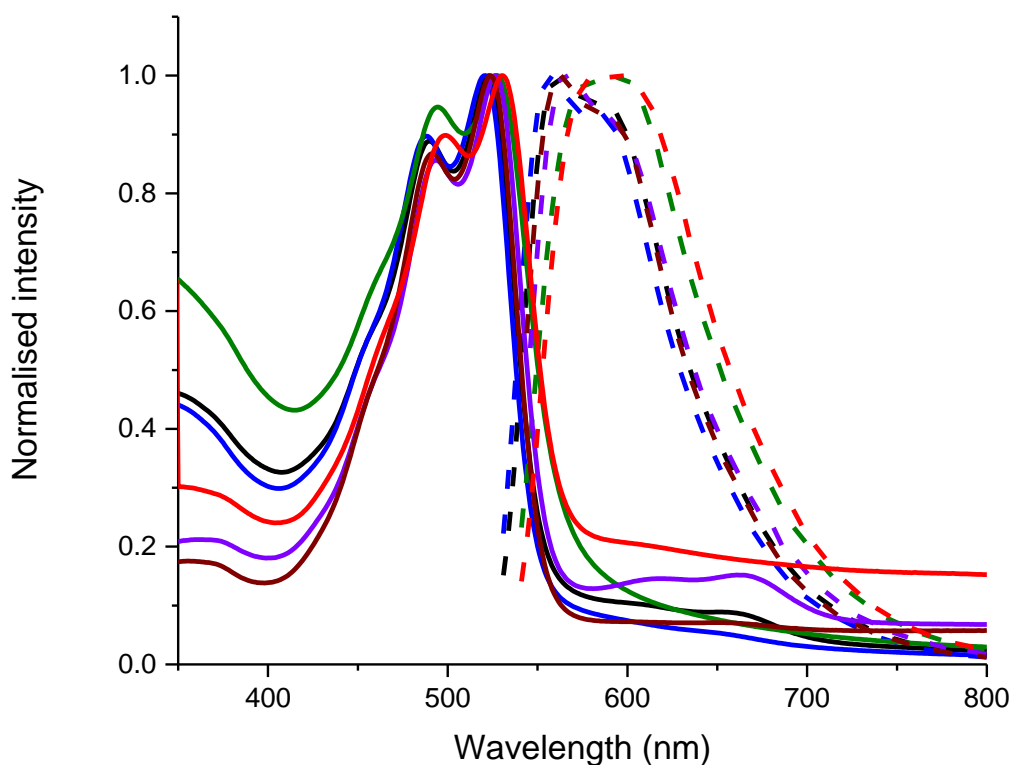
Figure S14.  $^{13}\text{C}$  NMR of 3-3.2PF<sub>6</sub> recorded in acetonitrile d<sub>3</sub>.



**Figure S15.** UV-visible absorbance (solid line) and emission (dashed line) spectra of 4-2.2PF<sub>6</sub> and 4-3.2PF<sub>6</sub> in different solvents. 4-2.2PF<sub>6</sub> in acetone (bergundy lines), 4-2.2PF<sub>6</sub> in acetonitrile (green lines), 4-2.2PF<sub>6</sub> in tetrahydrofuran (yellow lines). 4-3.2PF<sub>6</sub> in acetone (black lines), 4-3.2PF<sub>6</sub> in acetonitrile (red lines), 4-3.2PF<sub>6</sub> in tetrahydrofuran (blue lines).

**Table S2.** Absorption and fluorescence emission maxima ( $\lambda_{\text{abs/em}}$ ), Stokes shifts ( $\Delta\lambda$ ), and photoluminescence quantum yields ( $\phi$ ) of 4-2.2PF<sub>6</sub>, 4-3.2PF<sub>6</sub> in tetrahydrofuran (THF), in acetone and acetonitrile (MeCN).

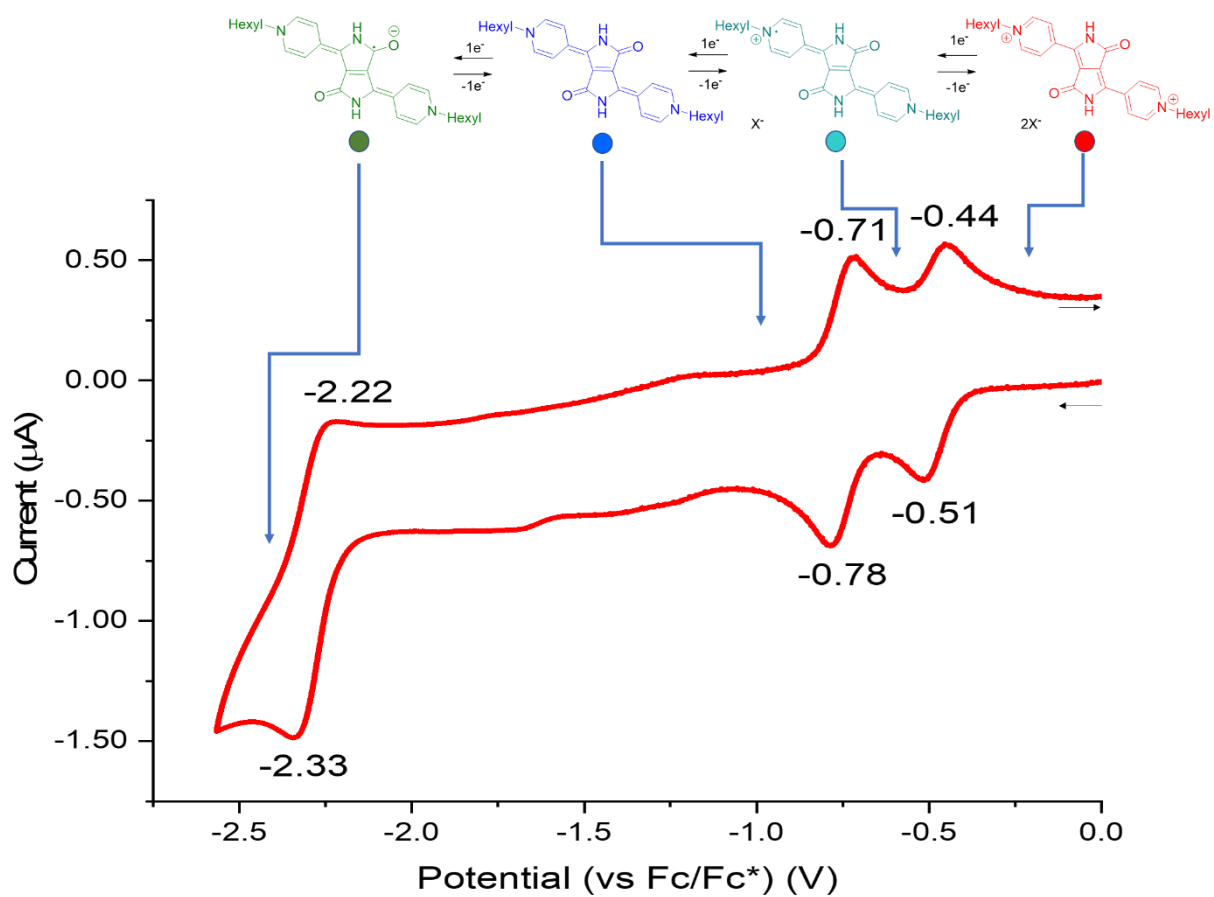
	Solvent	$\lambda_{\text{abs}}$ (nm)	$\lambda_{\text{ems}}$ (nm)	$\Delta\lambda$ (nm)	$\epsilon$ ( $\text{M}^{-1}\text{cm}^{-1}$ )	$\phi$
4-2.2PF <sub>6</sub>	THF	578	657	68	9,050	0.13
4-2.2PF <sub>6</sub>	Acetone	573	638	65	16,200	
4-2.2PF <sub>6</sub>	MeCN	570	628	58	16,900	
4-3.2PF <sub>6</sub>	THF	576	657	82	8,070	0.12
4-3.2PF <sub>6</sub>	Acetone	578	647	69	16,000	
4-3.2PF <sub>6</sub>	MeCN	574	640	66	14,000	



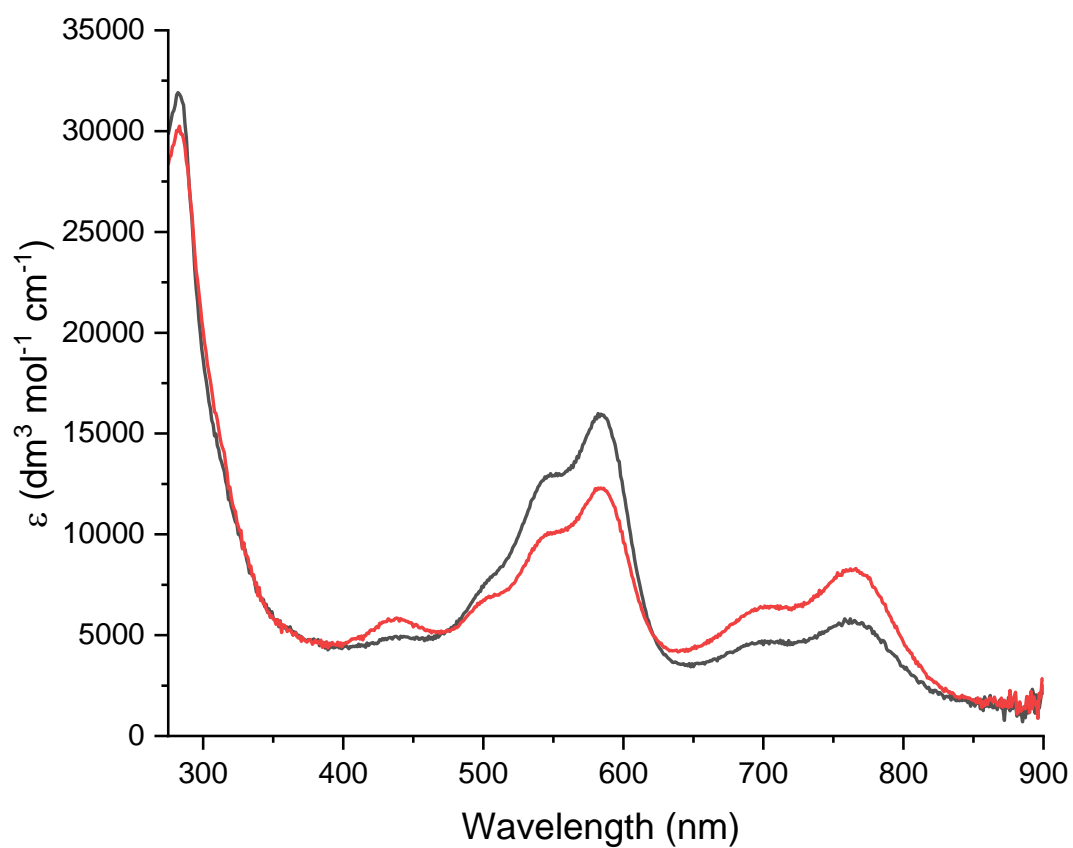
**Figure S16.** UV-visible absorbance (solid line) and emission (dashed line) spectra of 3-2.2PF<sub>6</sub> and 3-3.2PF<sub>6</sub> in different solvents. 3-2.2PF<sub>6</sub> in acetone (black lines), 3-2.2PF<sub>6</sub> in acetonitrile (blue lines), 3-2.2PF<sub>6</sub> in tetrahydrofuran (green lines). 3-3.2PF<sub>6</sub> in acetone (purple lines), 3-3.2PF<sub>6</sub> in acetonitrile (burgundy lines), 3-3.2PF<sub>6</sub> in tetrahydrofuran (red lines).

**Table S3.** Absorption and fluorescence emission maxima ( $\lambda_{\text{abs/em}}$ ), Stokes shifts ( $\Delta\lambda$ ), and photoluminescence quantum yields ( $\phi$ ) of 3-2.2PF<sub>6</sub>, 3-3.2PF<sub>6</sub> in tetrahydrofuran (THF), in acetone and acetonitrile (MeCN).

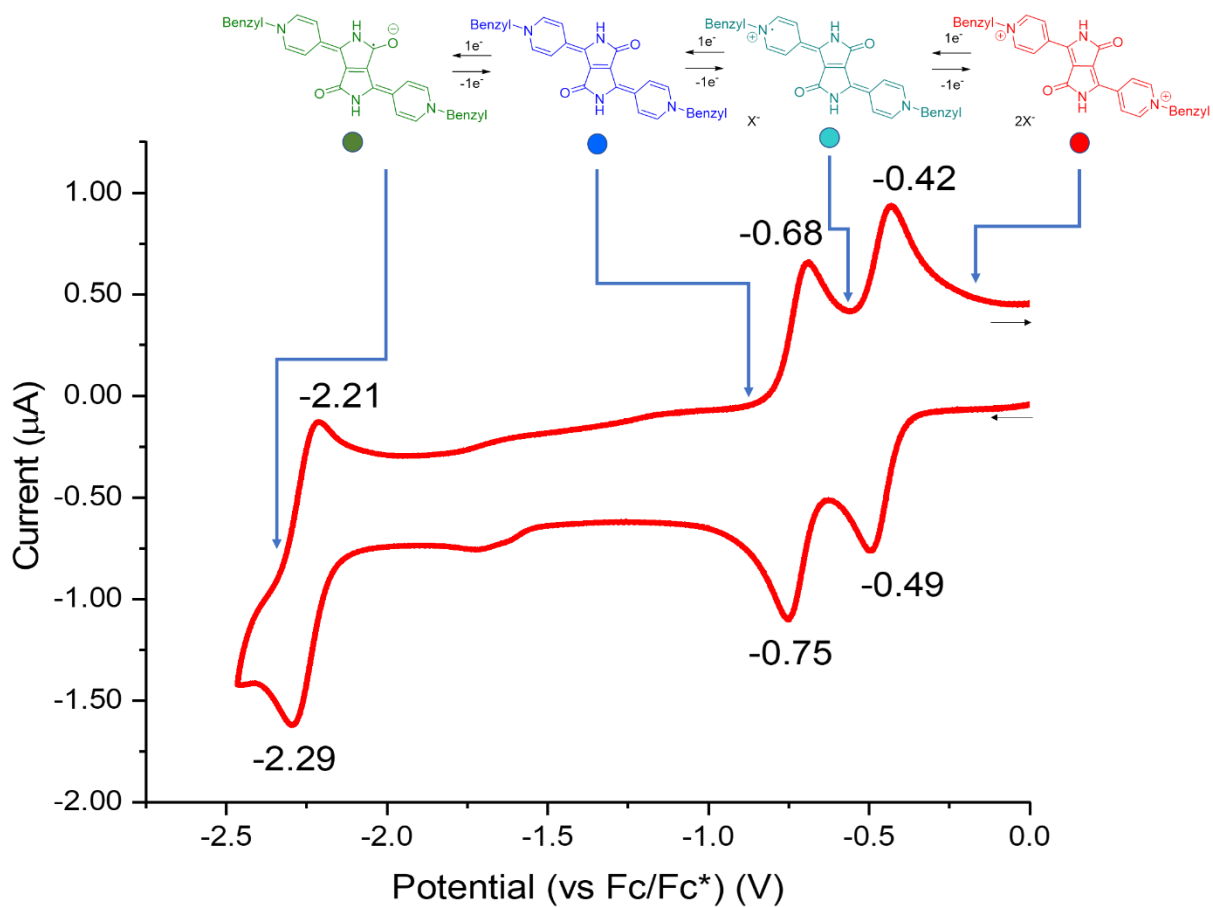
	Solvent	$\lambda_{\text{abs}}$ (nm)	$\lambda_{\text{ems}}$ (nm)	$\Delta\lambda$ (nm)	$\epsilon$ (M <sup>-1</sup> cm <sup>-1</sup> )	$\phi$
3-2.2PF <sub>6</sub>	THF	528	596	68		
3-2.2PF <sub>6</sub>	Acetone	523	562	39	13,883	
3-2.2PF <sub>6</sub>	MeCN	521	557	35	12,990	0.55
3-3.2PF <sub>6</sub>	THF	531	584	53		
3-3.2PF <sub>6</sub>	Acetone	536	567	41	12770	
3-3.2PF <sub>6</sub>	MeCN	524	563	39	12500	0.59



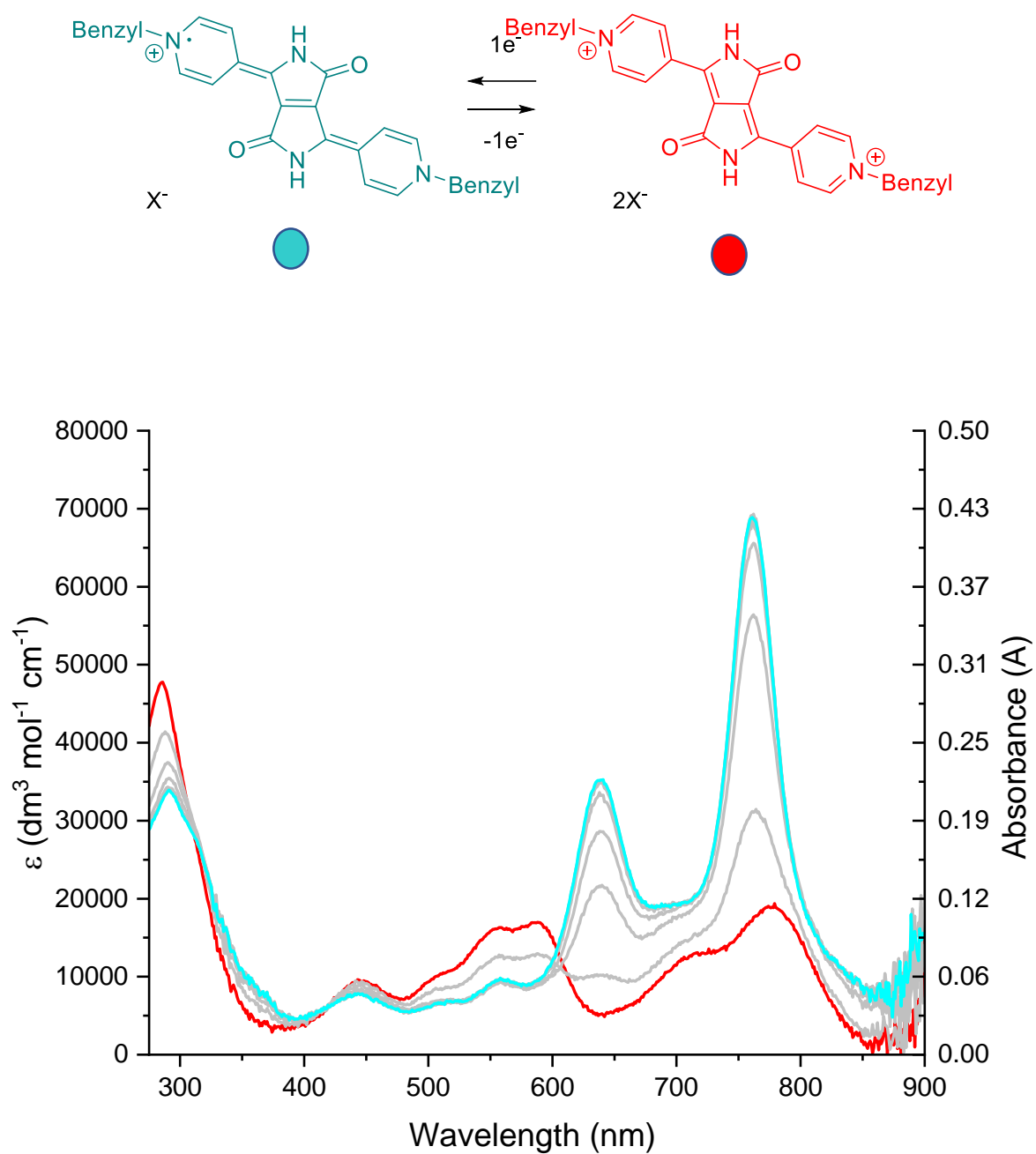
**Figure S17** Cyclic voltammetry of 4-2.2PF<sub>6</sub> on a glassy carbon electrode in DMF solution with [n-Bu<sub>4</sub>N][PF<sub>6</sub>] (0.2 M) as supporting electrolyte.



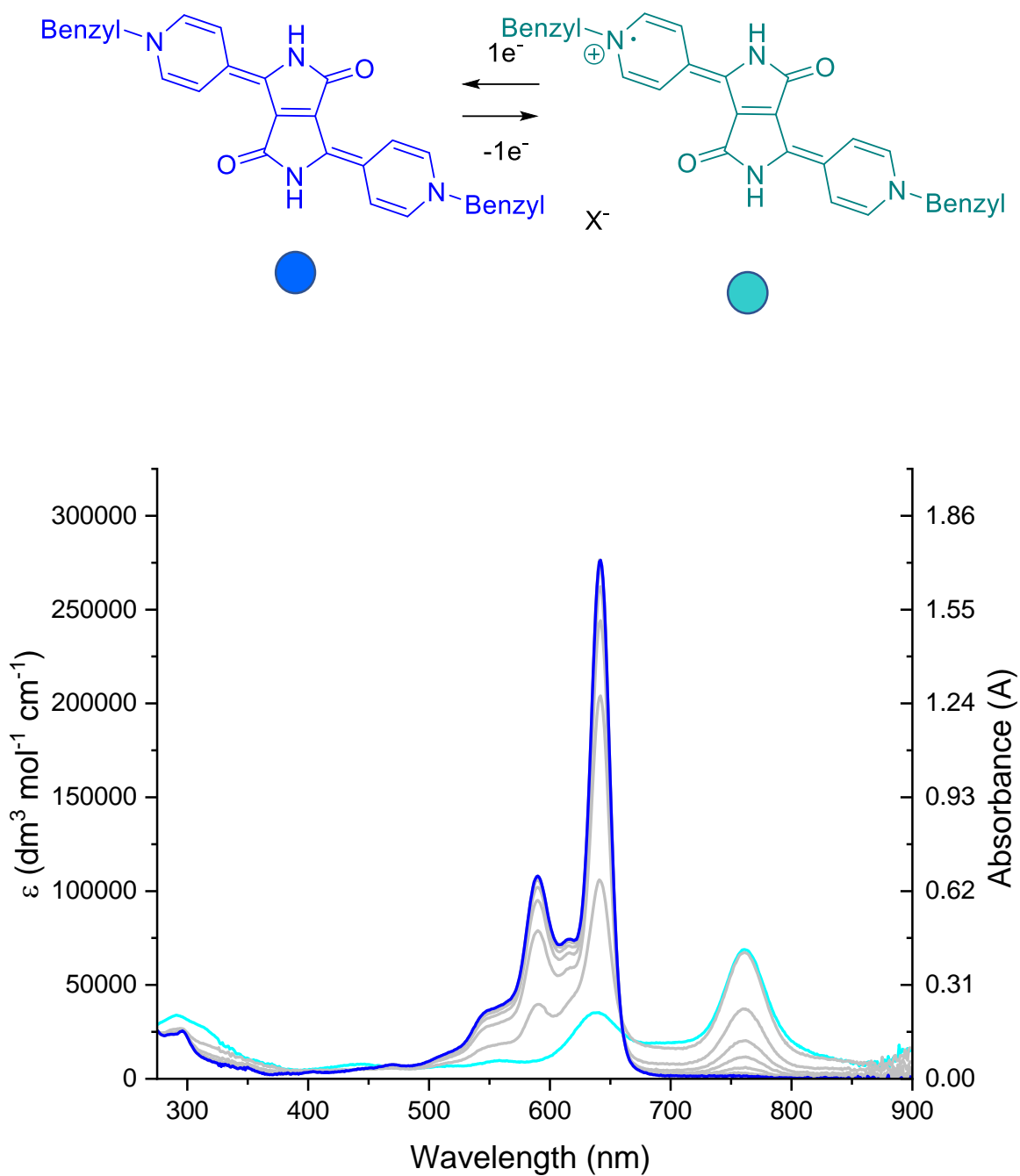
**Figure S18.** UV-visible absorption spectra of 4-2.2PF<sub>6</sub> (first scan) and after the oxidation cycle (final scan). Spectra were recorded in DMF containing [*n*-Bu<sub>4</sub>N][PF<sub>6</sub>] (0.2 M) as the supporting electrolyte at 273 K.



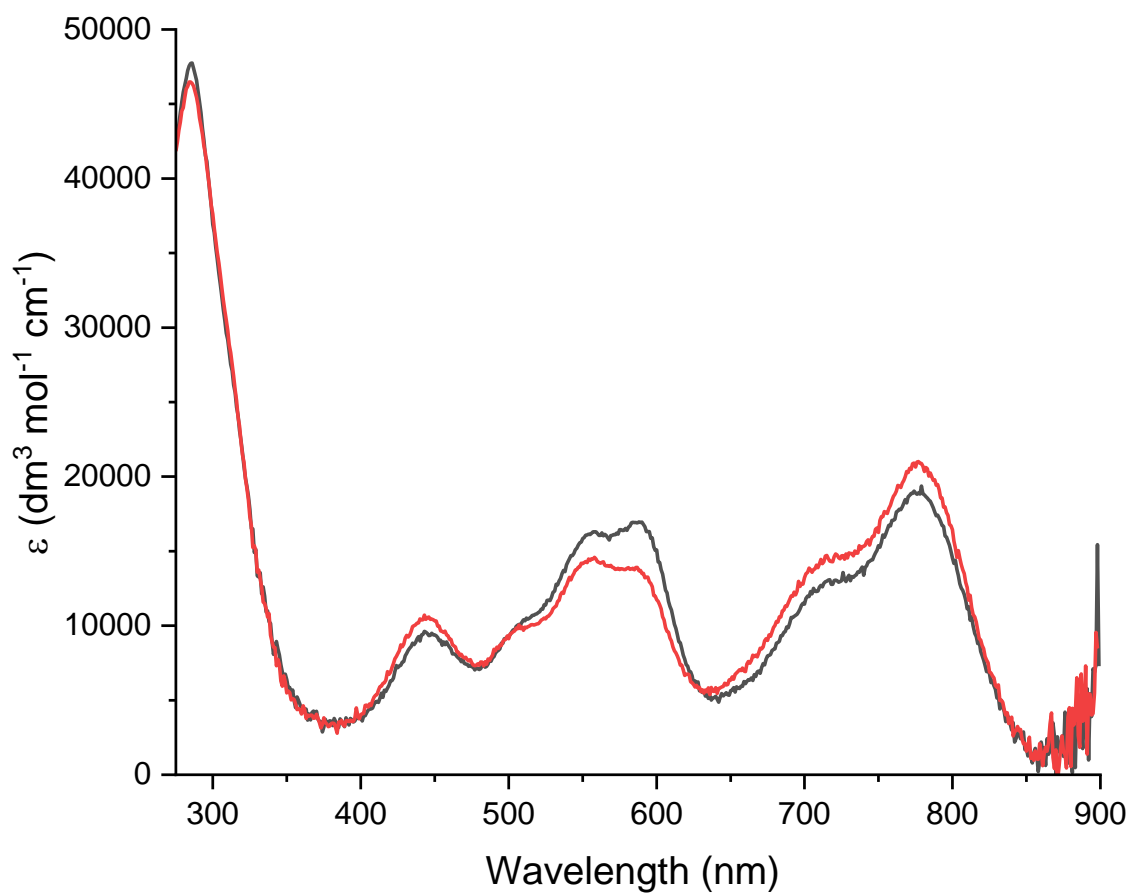
**Figure S19** Cyclic voltammetry of 4-3.2PF<sub>6</sub> on a glassy carbon electrode in DMF solution with [n-Bu<sub>4</sub>N][PF<sub>6</sub>] (0.2 M) as supporting electrolyte.



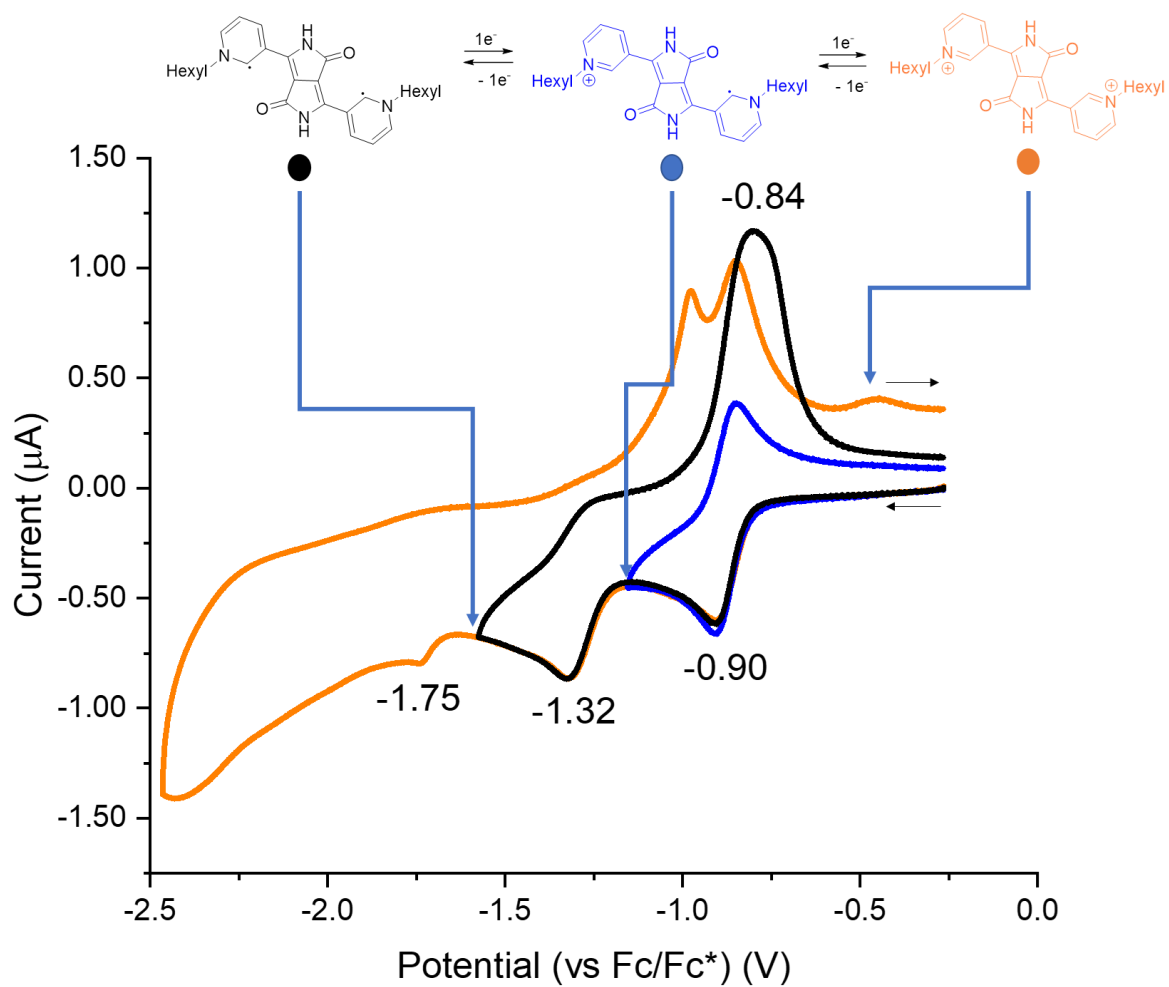
**Figure S20.** UV-visible absorption monitoring of the first reduction process of 4-3.2PF<sub>6</sub>, Red line 4-3.2PF<sub>6</sub>, cyan line 4-3.2PF<sub>6</sub>. Colored lines show  $\epsilon$ , gray lines correspond to absorbance. Spectra were recorded in DMF containing [n-Bu<sub>4</sub>N][PF<sub>6</sub>] (0.2 M) as the supporting electrolyte at 273 K.



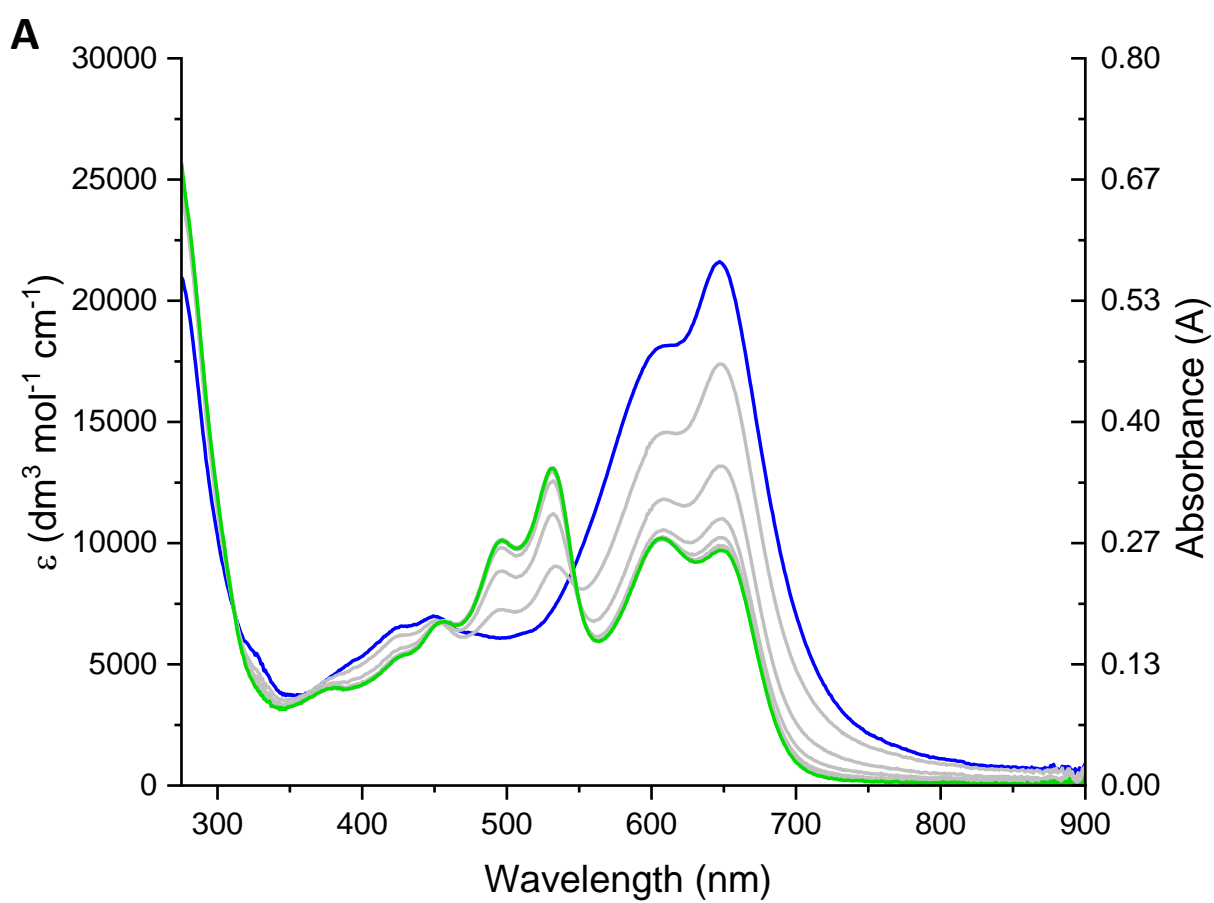
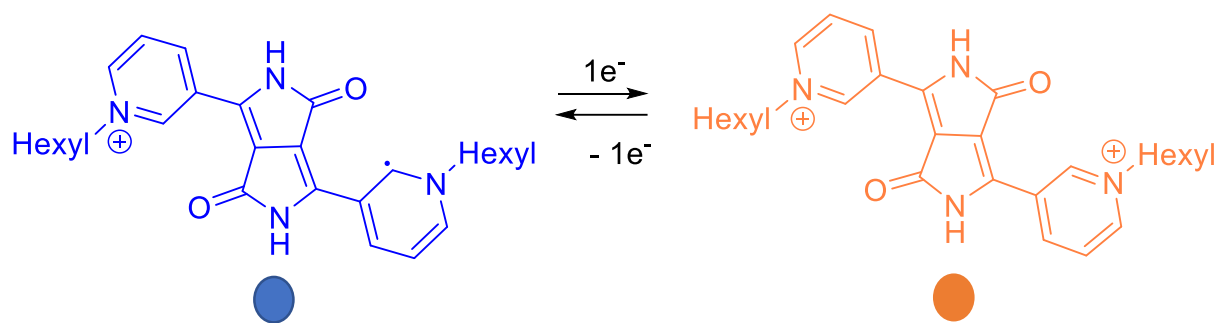
**Figure S21.** UV-visible absorption monitoring the second reduction process of  $4\text{-}\mathbf{3}\cdot 2\text{PF}_6^+$ . Cyan line  $4\text{-}\mathbf{3}\cdot 2\text{PF}_6$ ; blue line  $4\text{-}\mathbf{3}\cdot 2\text{PF}_6^+$ . Colored lines show  $\epsilon$ , gray lines correspond to absorbance. Spectra were recorded in DMF containing  $[n\text{-Bu}_4\text{N}][\text{PF}_6]$  (0.2 M) as the supporting electrolyte at 273 K.

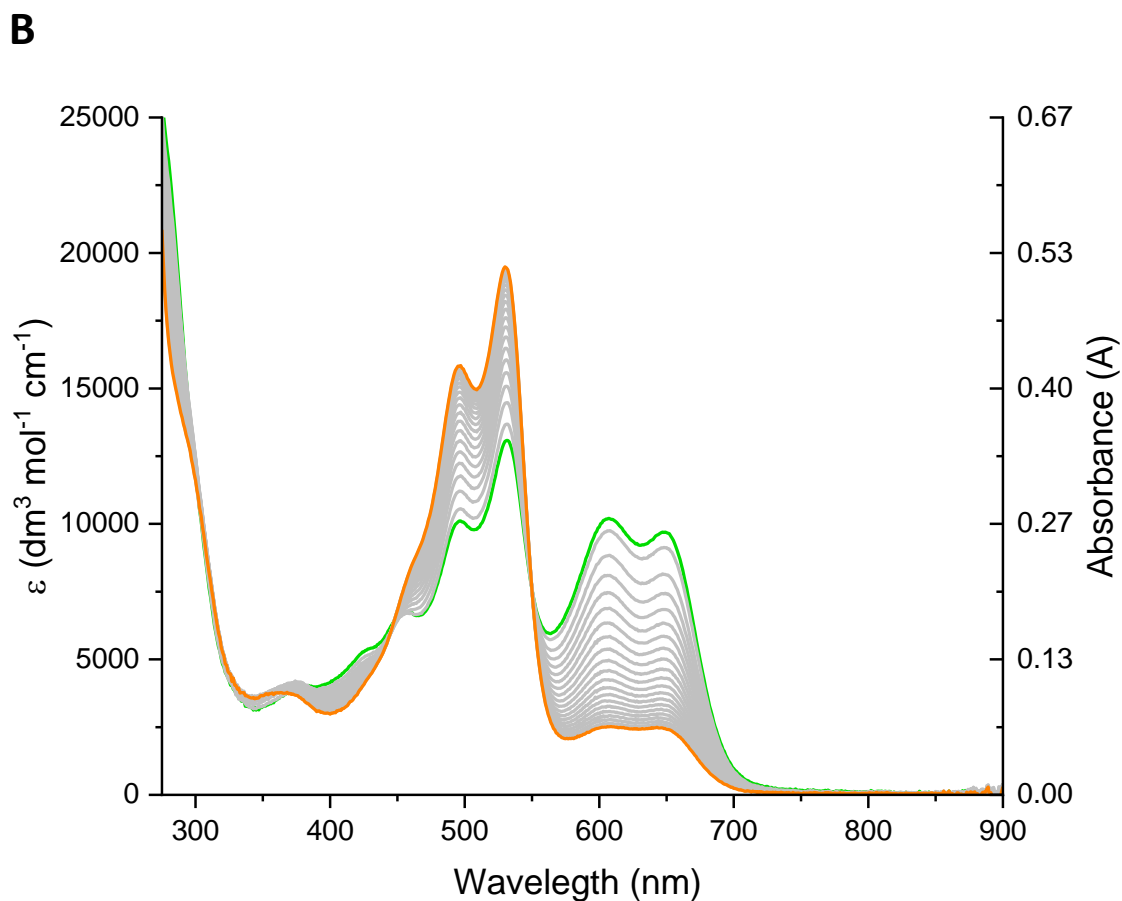


**Figure S22.** UV-visible absorption spectra of 4-3.2PF<sub>6</sub> (first scan) and after the oxidation cycle (final scan). Spectra were recorded in DMF containing [n-Bu<sub>4</sub>N][PF<sub>6</sub>] (0.2 M) as the supporting electrolyte at 273 K.

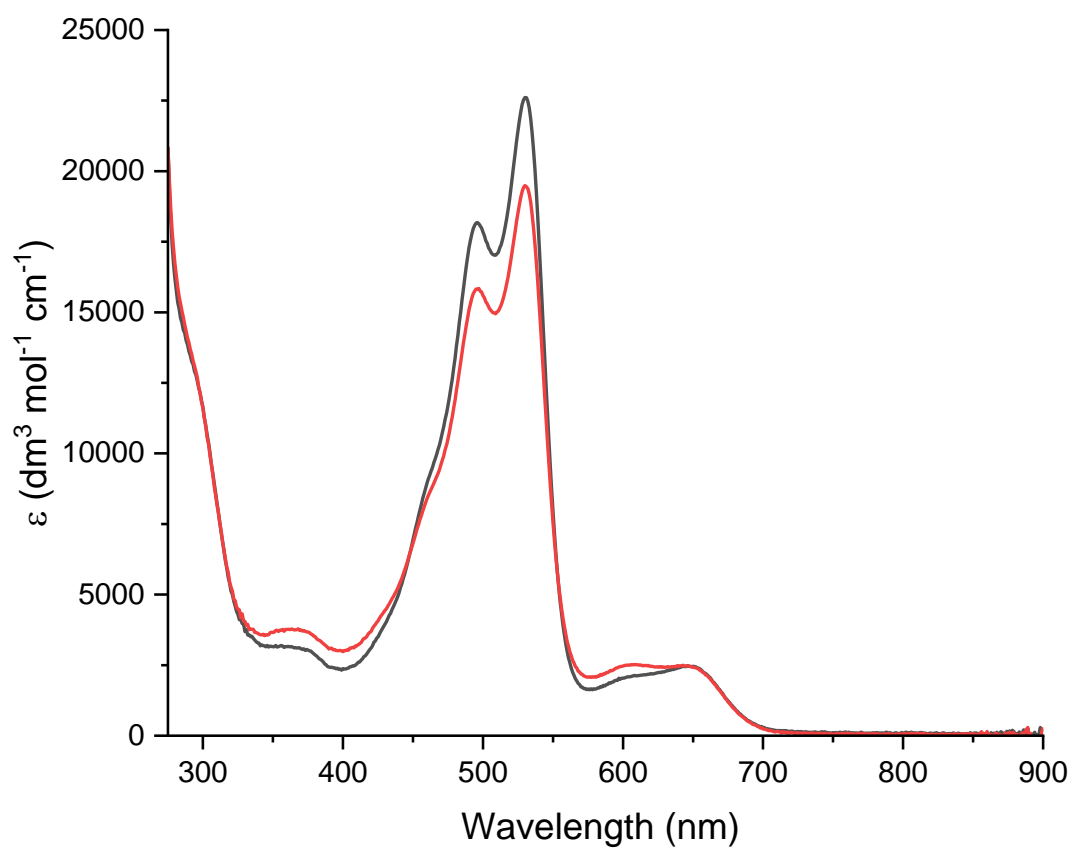


**Figure S23** Cyclic voltammety of 3-2.PF<sub>6</sub> on a glassy carbon electrode in DMF solution with [n-Bu<sub>4</sub>N][PF<sub>6</sub>] (0.2M) as supporting electrolyte.

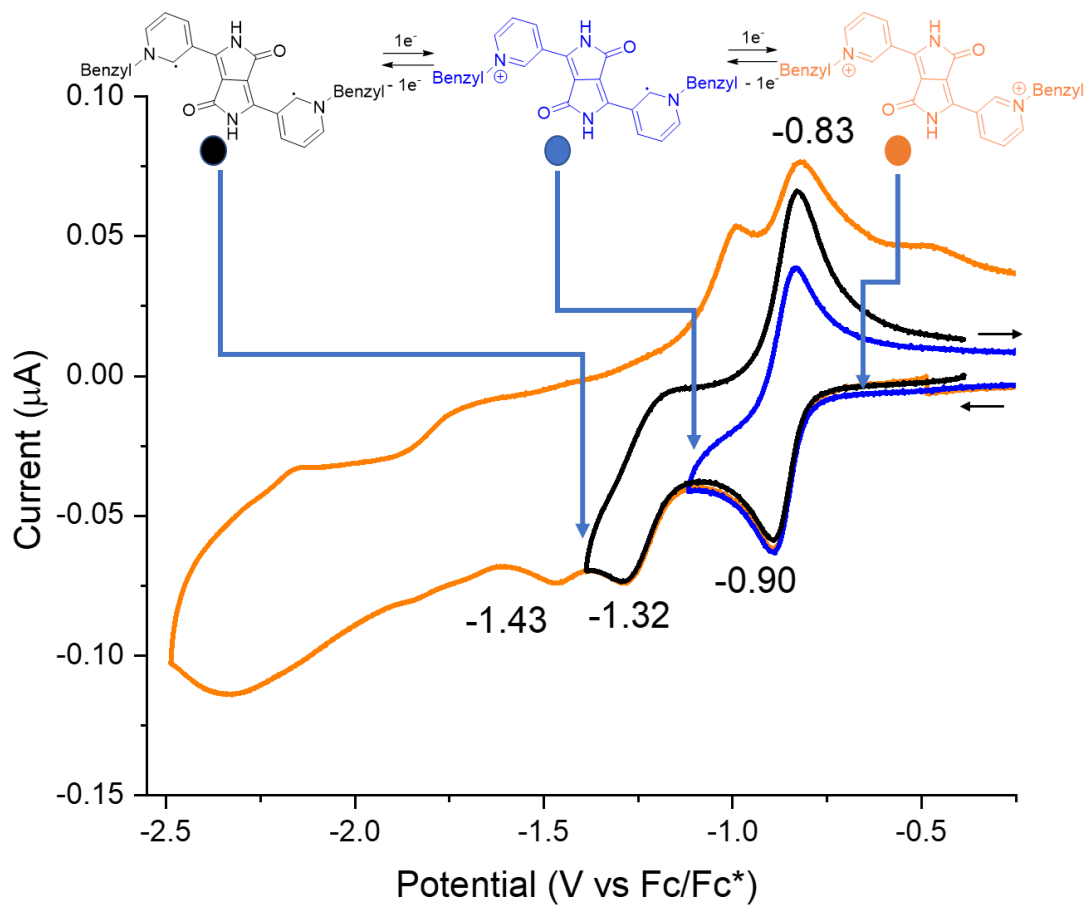




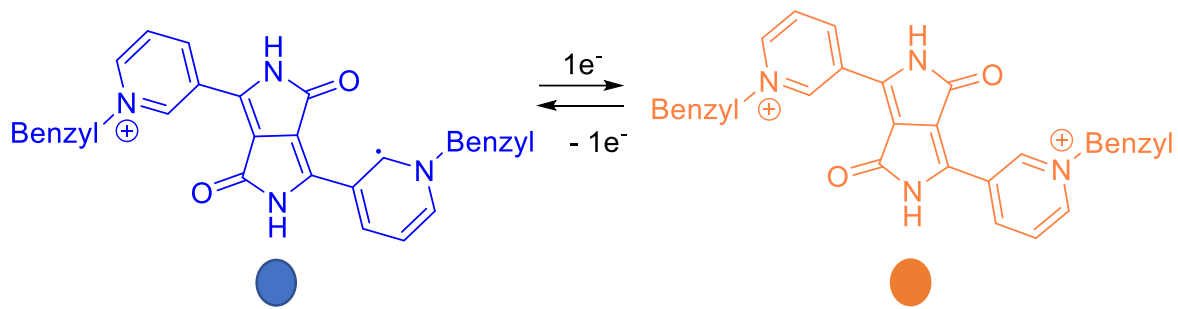
**Figure S24.** UV-visible monitoring **A** re-oxidation of  $3\text{-}2\text{-PF}_6^-$  (Blue line) having stable ratio between reduced and oxidized species (green line). **B** from the stable ratio between reduced and oxidated species (green line) return to the starting material  $3\text{-}2\text{-}2\text{PF}_6$  (Orange line) which required additional positive potential. Colored lines correspond to  $\epsilon$ , gray lines show absorbance. Spectra were recorded in DMF containing  $[n\text{-Bu}_4\text{N}][\text{PF}_6]$  (0.2 M) as the supporting electrolyte at 273 K.



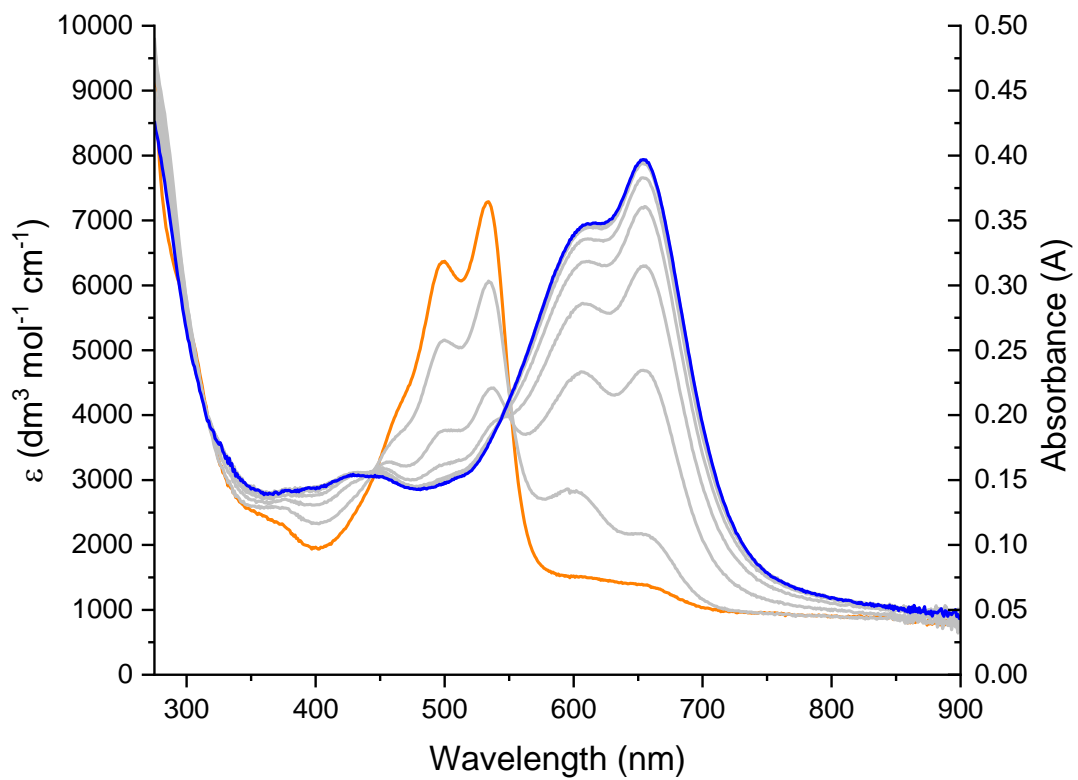
**Figure S25.** UV-visible absorption spectra of 3-2.2PF<sub>6</sub> (first scan) and after the oxidation cycle (final scan). Spectra were recorded in DMF containing [*n*-Bu<sub>4</sub>N][PF<sub>6</sub>] (0.2 M) as the supporting electrolyte at 273 K.

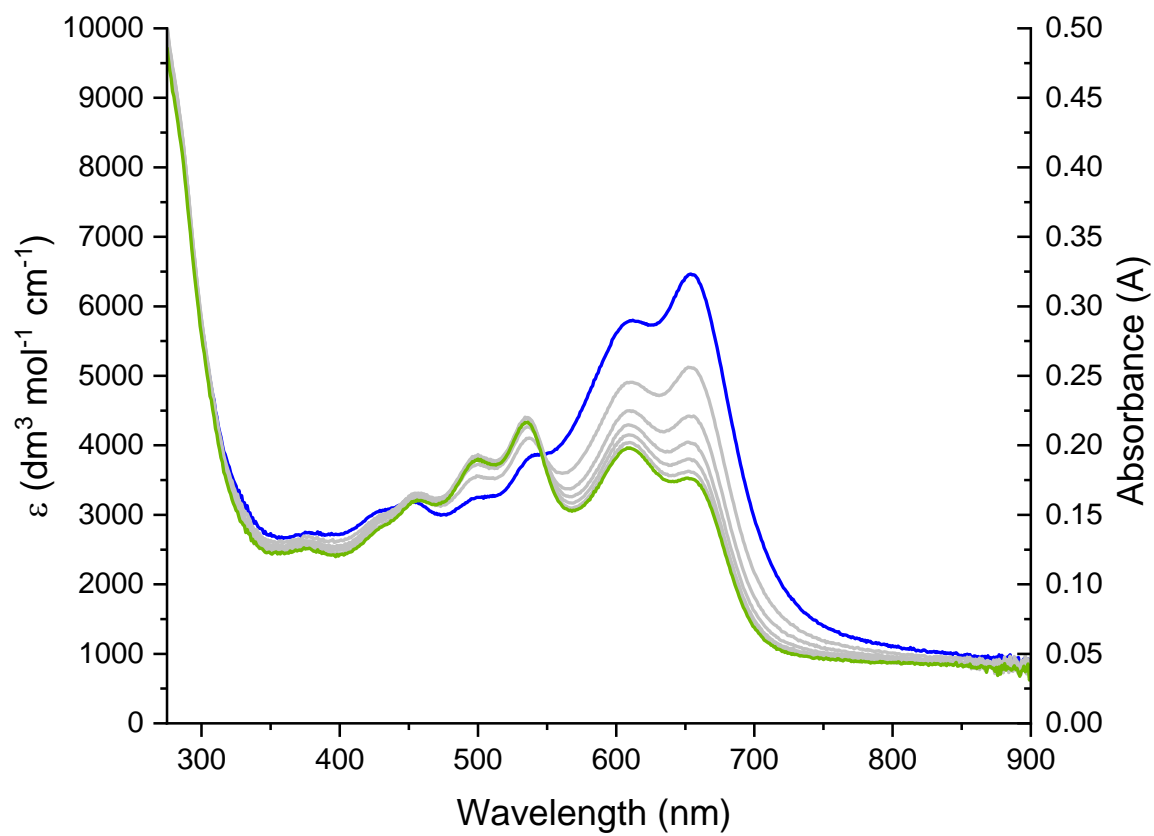


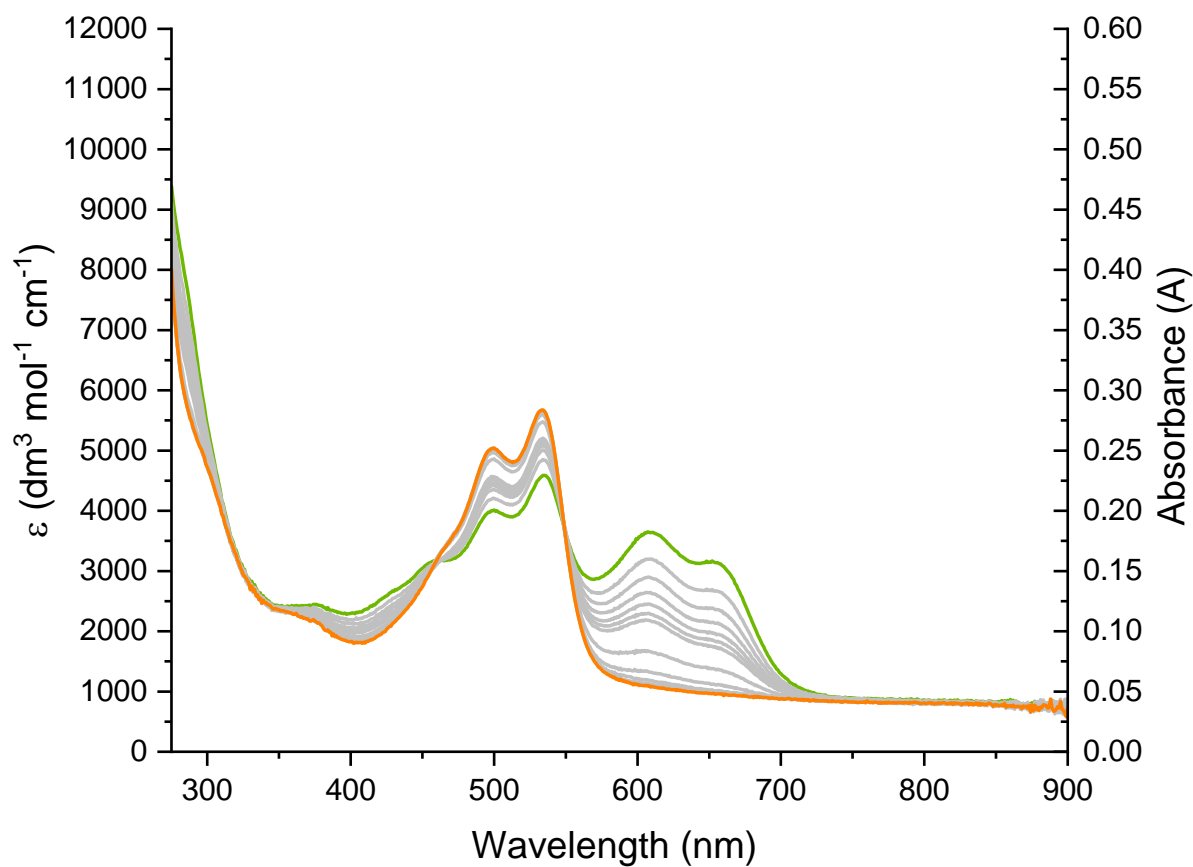
**Figure S26** Cyclic voltammetry of 3-3.PF<sub>6</sub> on a glassy carbon electrode in DMF solution with [n-Bu<sub>4</sub>N][PF<sub>6</sub>] (0.2M) as supporting electrolyte.



**A**



**B**

**C**

**Figure S27.** UV-visible absorption monitoring of **A** the reduction of 3-3.2PF<sub>6</sub> (orange line) to 3-3.PF<sub>6</sub><sup>-</sup> (blue line). **B** re-oxidation of 3-3.PF<sub>6</sub><sup>-</sup> (blue line) having stable ratio between reduced and oxidized species (green line). **C** from the ratio between reduced and oxidized species (green line) return to the starting material 3-3.2PF<sub>6</sub> (Orange line) which required additional positive potential. Colored lines correspond to  $\epsilon$ , gray lines show absorbance. Spectra were recorded in DMF containing [*n*-Bu<sub>4</sub>N][PF<sub>6</sub>] (0.2 M) as the supporting electrolyte at 273 K.

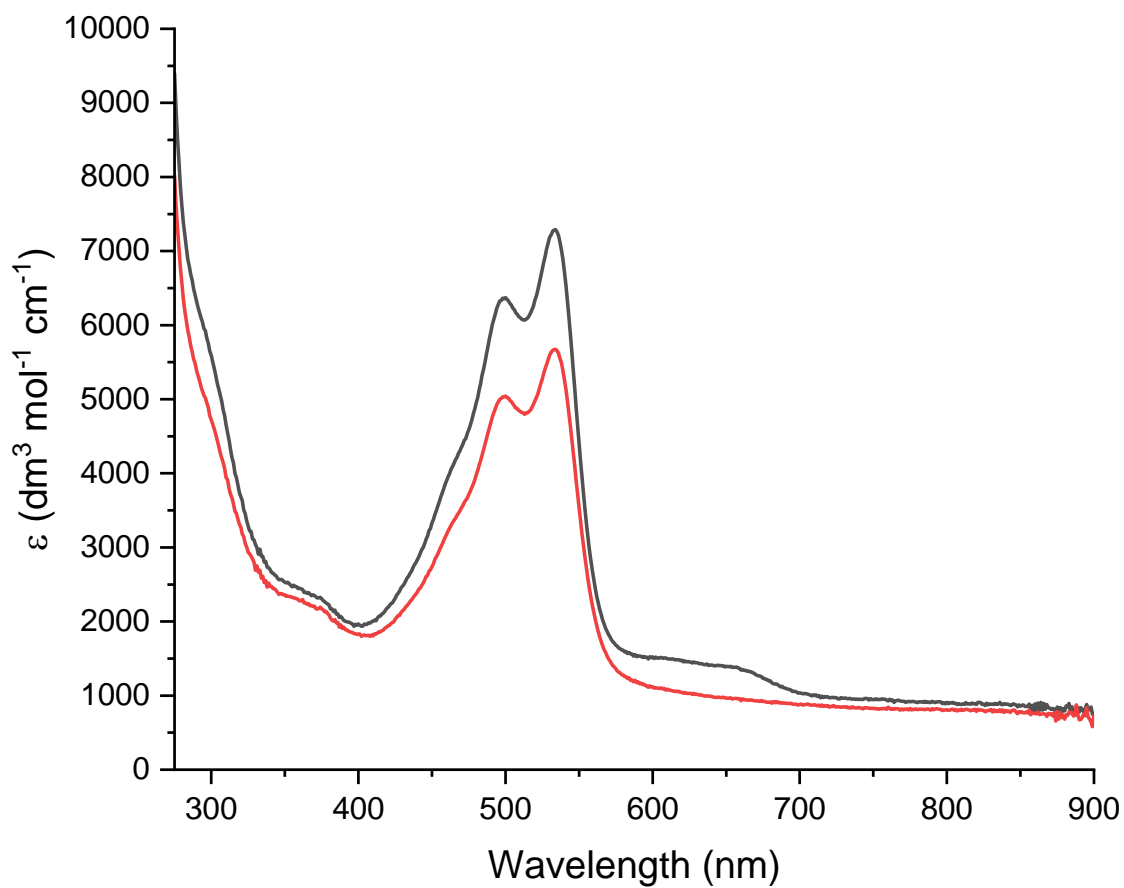


**Figure S28.** UV-visible absorption spectra of 3-3.2PF<sub>6</sub> (first scan) and after the oxidation cycle (final scan). Spectra were recorded in DMF containing [*n*-Bu<sub>4</sub>N][PF<sub>6</sub>] (0.2 M) as the supporting electrolyte at 273 K.

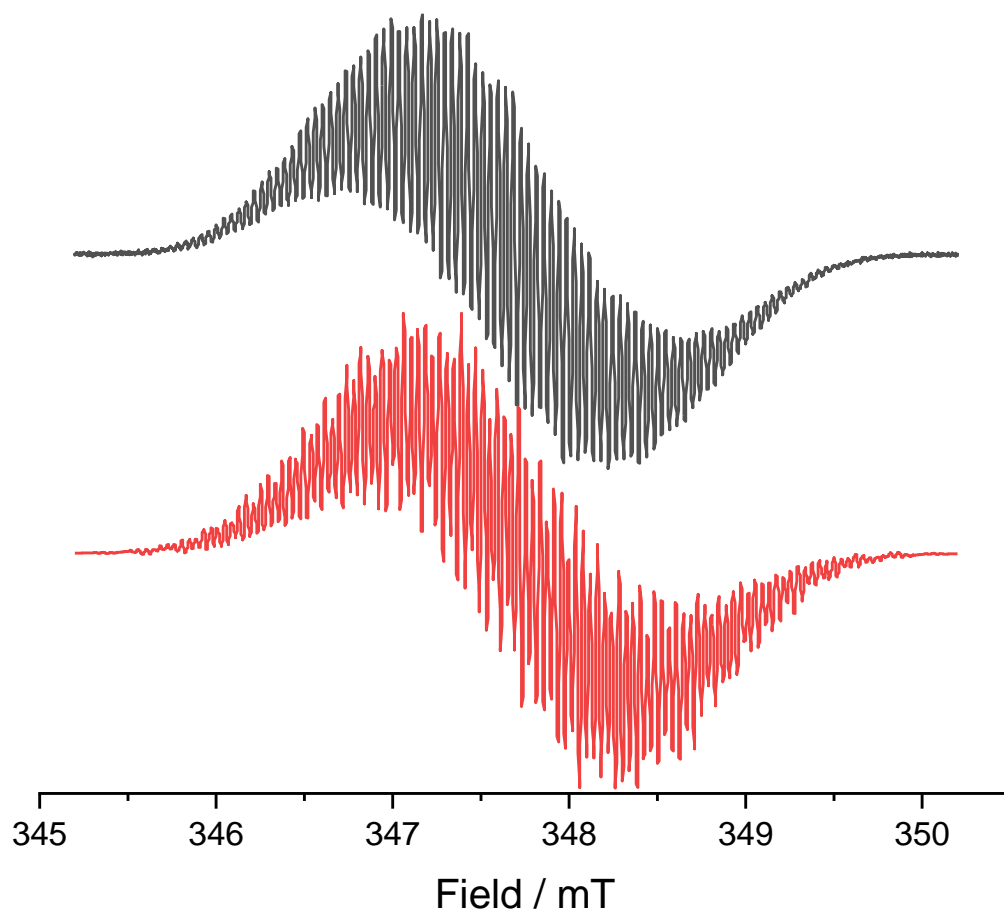


**Figure S29** Experimental (top) and simulated (bottom) EPR spectra of singly reduced 4-**3**.2PF<sub>6</sub>. In DMF containing [n-Bu<sub>4</sub>N][PF<sub>6</sub>] (0.2 M) as the supporting electrolyte at room temperature. Simulation: H coupling 0.2497, 0.1931, 0.1675, 0.0431; N coupling 0.3303, 0.3195.

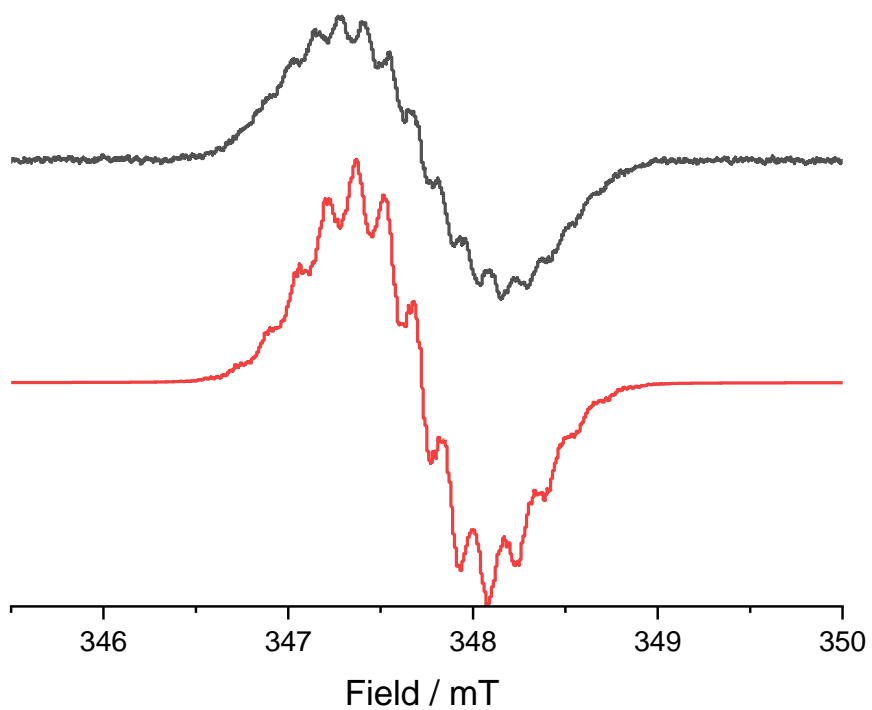


**Figure S30** Experimental (top) and simulated (bottom) EPR spectra of singly reduced 4-2.PF<sub>6</sub> in DMF containing [n-Bu<sub>4</sub>N][PF<sub>6</sub>] (0.2 M) as the supporting electrolyte at room temperature. Simulation: H coupling 0.1626, 0.1380, 0.1380, 0.0280; N coupling 0.1697, 0.0643.

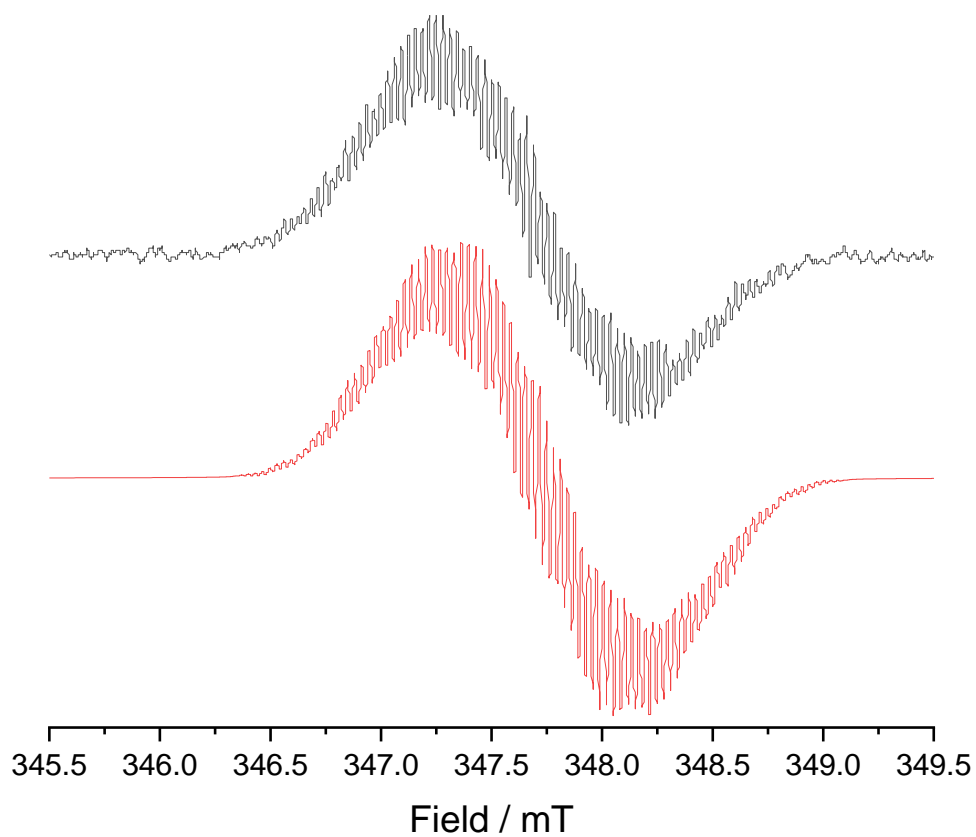


**Figure S31** Experimental (top) and simulated (bottom) EPR spectra of singly reduced 3-3.2PF<sub>6</sub> in DMF containing [n-Bu<sub>4</sub>N][PF<sub>6</sub>] (0.2 M) as the supporting electrolyte at room temperature. Simulation: H coupling 0.1847, 0.1696, 0.1350, 0.2950, 0.0275; N coupling 0.2587, 0.0639.

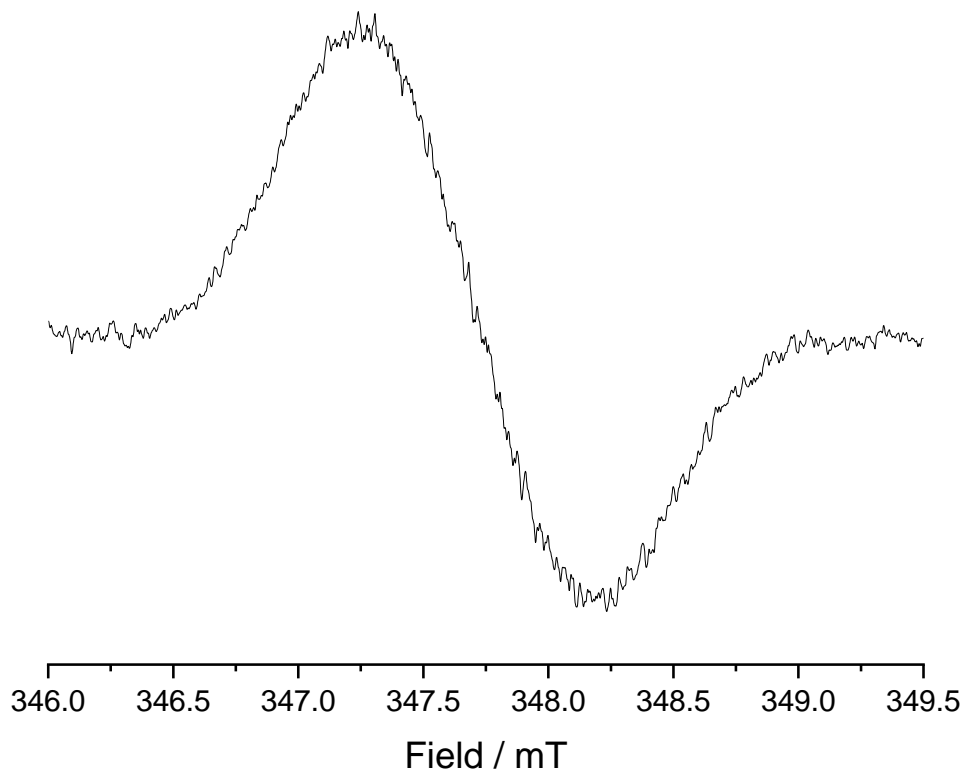


**Figure S32** Experimental EPR spectrum of singly reduced 3-2.PF<sub>6</sub> in DMF containing [n-Bu<sub>4</sub>N][PF<sub>6</sub>] (0.2 M) as the supporting electrolyte at room temperature.

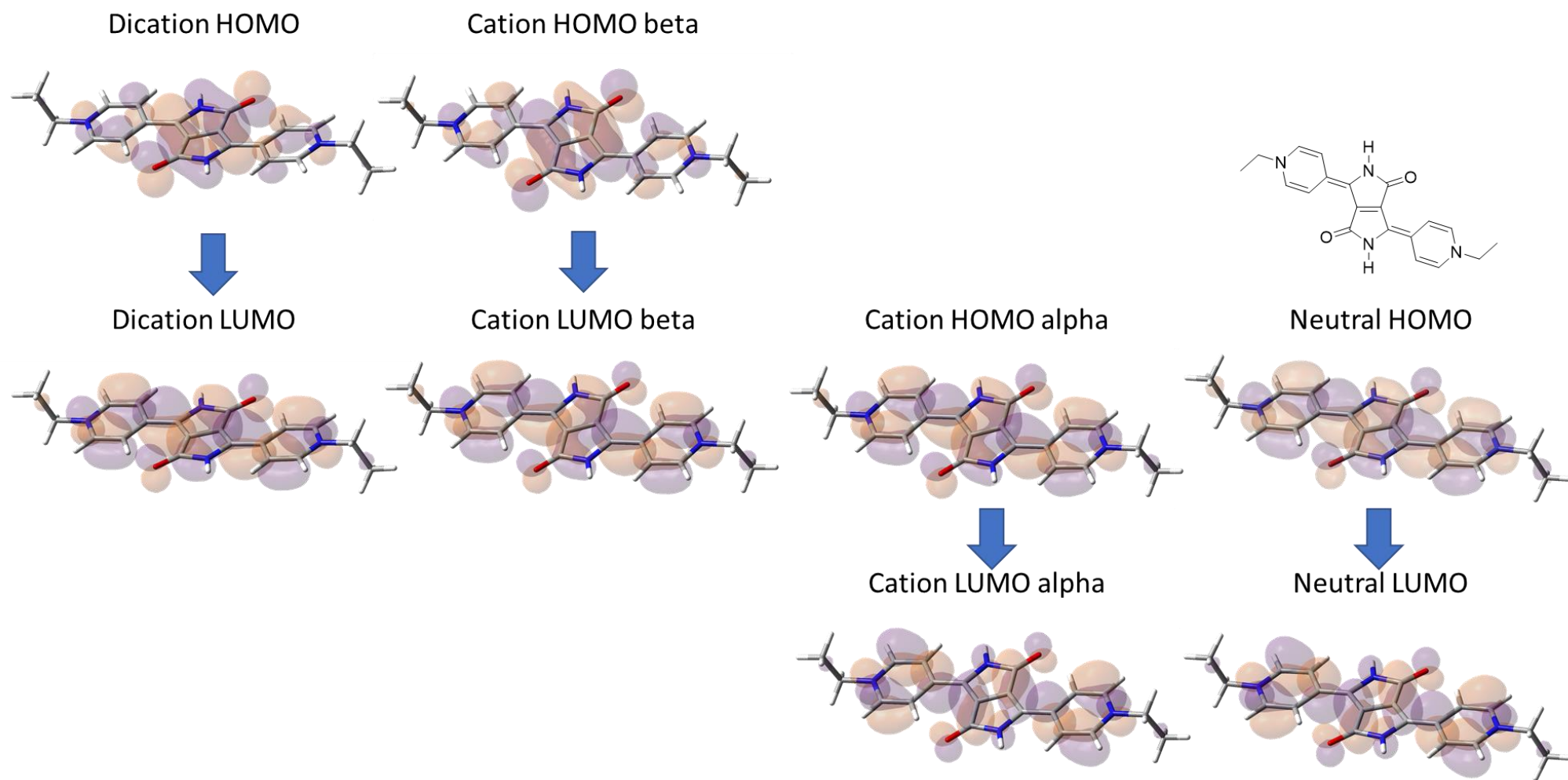


**Figure S33.** Structures of HOMO, SOMO, LUMO of 4-2<sup>+</sup>

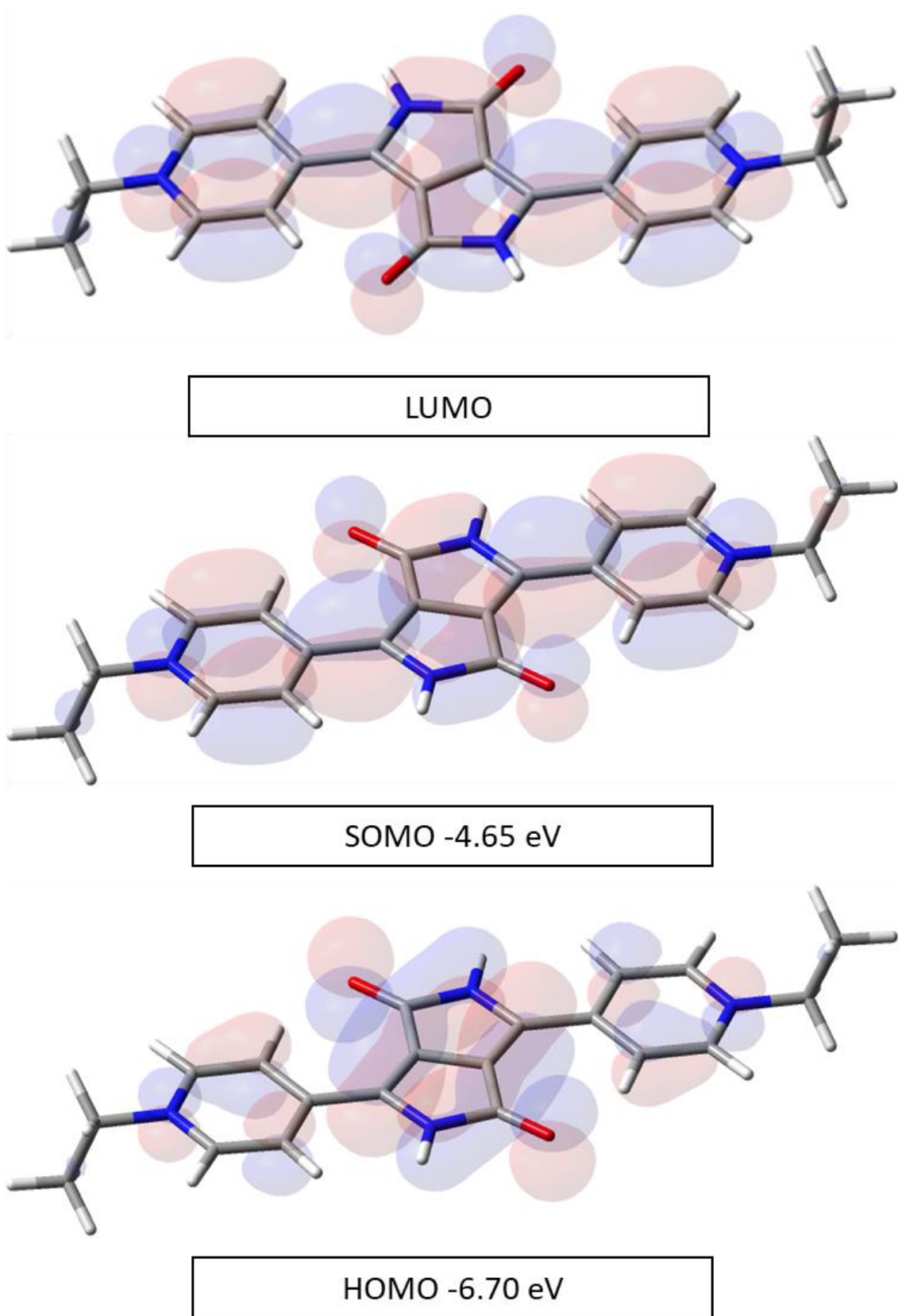
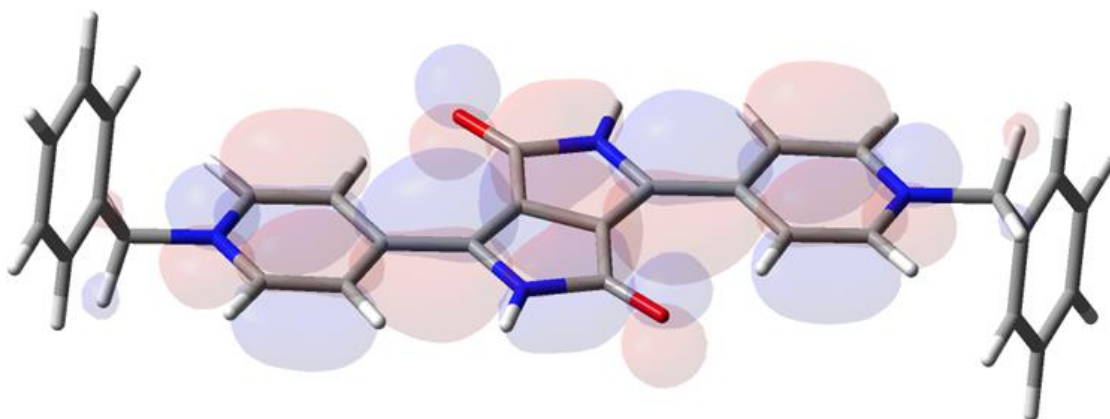
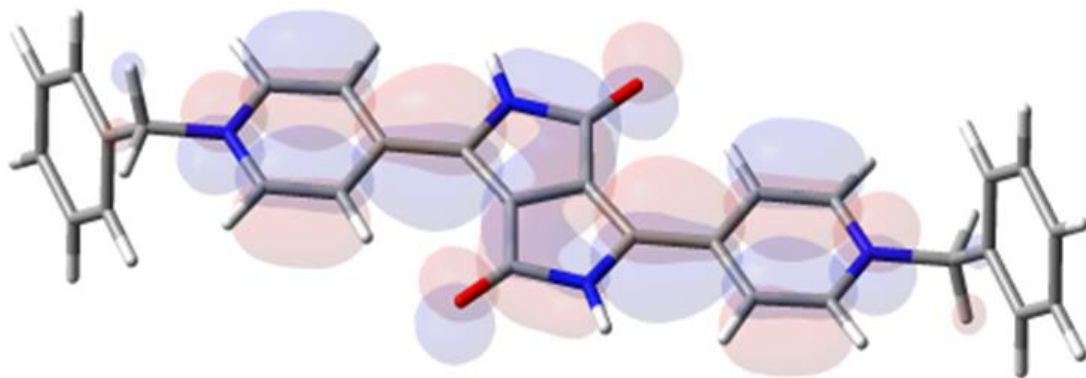


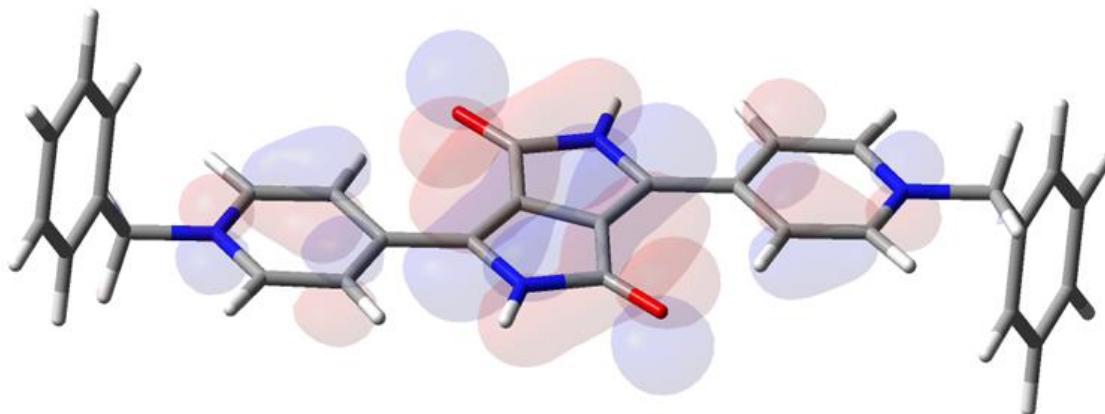
**Figure S34** Structures of HOMO, SOMO, LUMO of 4-2<sup>+</sup> and associated energies in eV.



LUMO

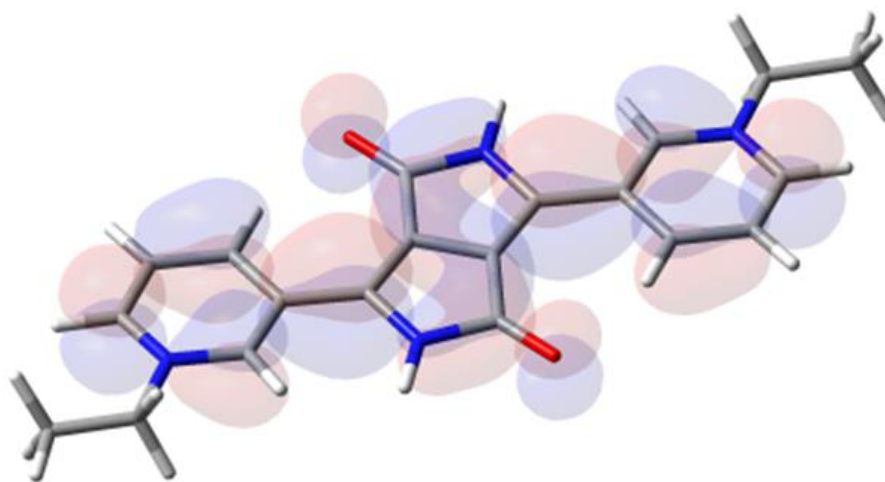


SOMO -4.64 eV

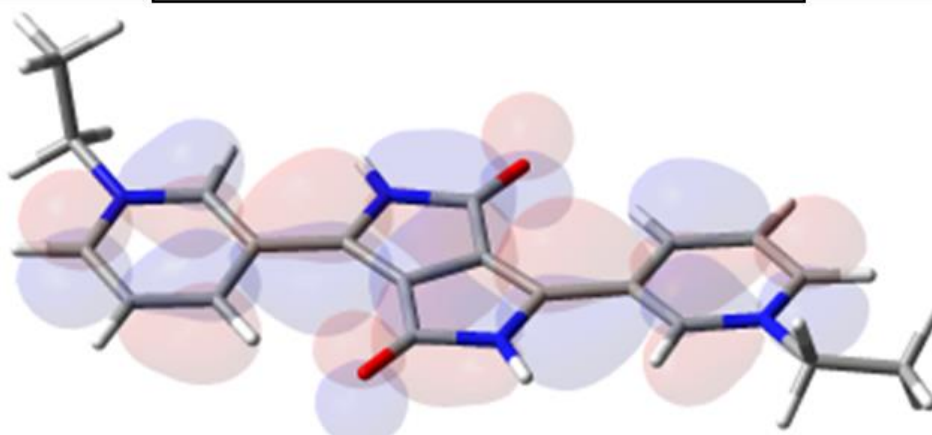


HOMO -6.70 eV

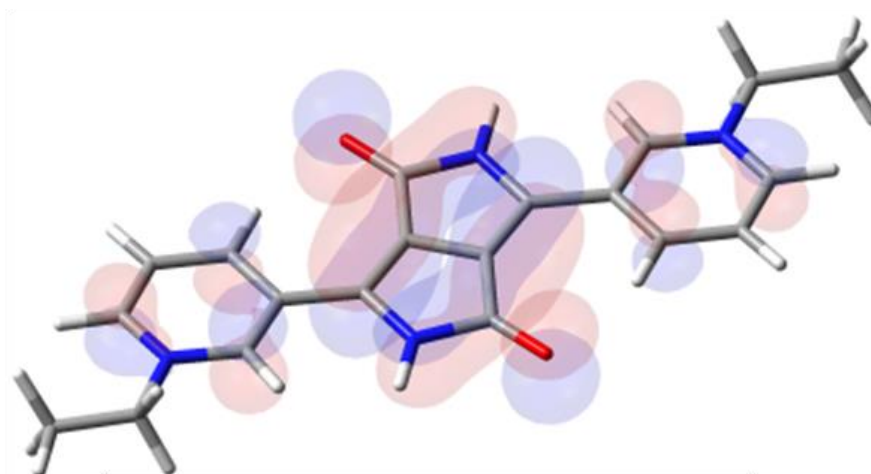
**Figure S35** Structures of HOMO, SOMO, LUMO of  $4\text{-}3^{2+}$  and associated energies in eV.



LUMO



SOMO -4.19 eV



HOMO -6.54 eV

**Figure S36** Structures of HOMO, SOMO, LUMO of  $3\text{-}2^{2+}$  and associated energies in eV.

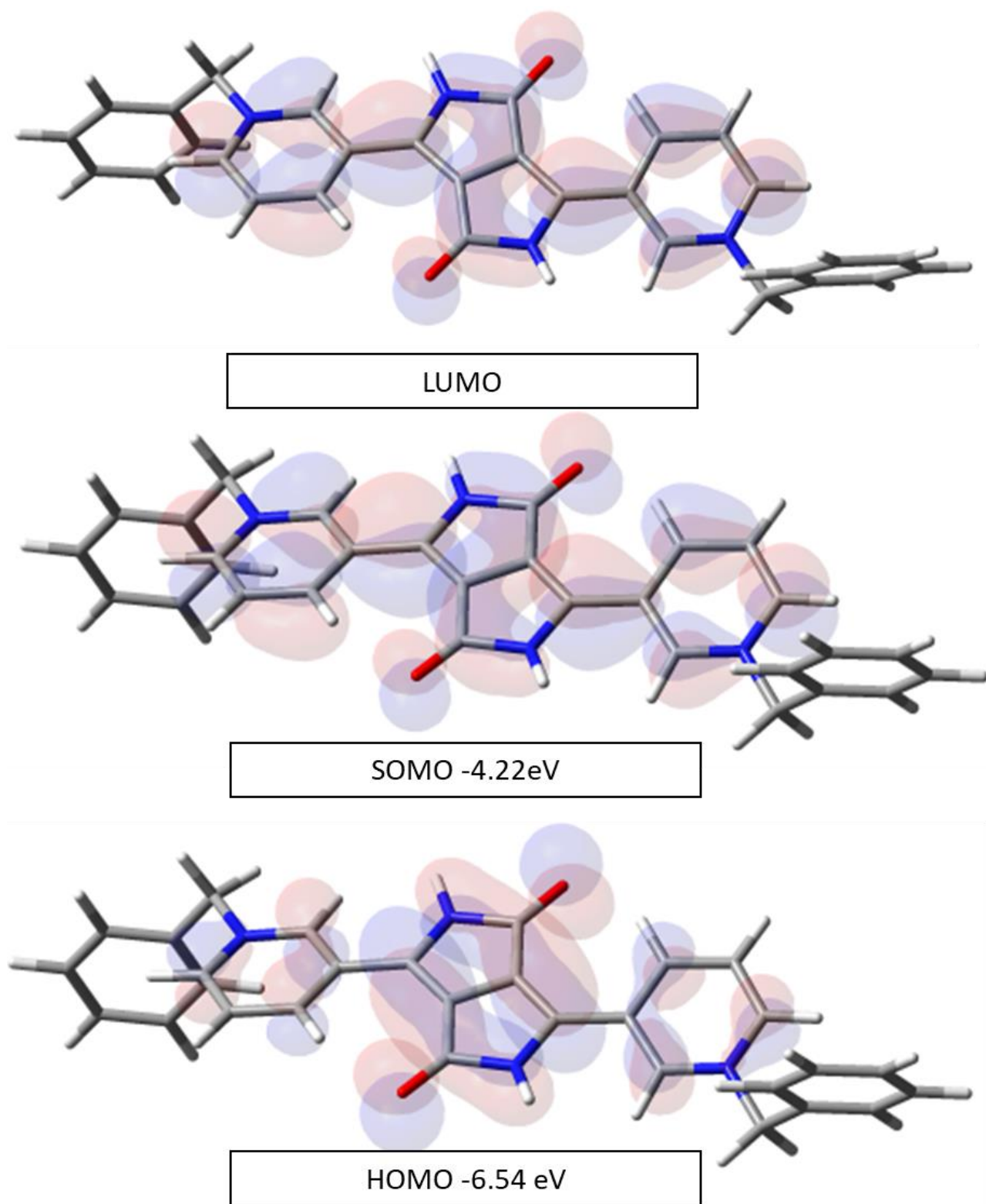


**Figure S37** Structures of HOMO, SOMO, LUMO of 3-3<sup>2+</sup> and associated energies in eV.

**Table S4.** Experimental and calculated HOMO-LUMO energy levels of 4-2<sup>+</sup>, 4-3<sup>+</sup>, 3-2<sup>+</sup>, 3-3<sup>+</sup> in eV

Compound	Experimental HOMO*	Calculated HOMO	Experimental LUMO	Calculated LUMO**	Optical Energy gap (E <sub>g</sub> )
4-2 <sup>+</sup>	-6.36 eV	-6.70 eV	-4.33 eV	-4.59 eV	2.03 eV
4-3 <sup>+</sup>	-6.33 eV	-6.70 eV	-4.35 eV	-4.61 eV	1.98 eV
3-2 <sup>+</sup>	-6 eV	-6.54 eV	-3.93 eV	-4.15 eV	2.07 eV
3-3 <sup>+</sup>	-5.96 eV	-6.54 eV	-3.94 eV	-4.16 eV	2.02 eV

\* Experimental HOMO calculated by difference between LUMO and the Optical Energy gap.

\*\* Calculated LUMO levels from B3LYP run.

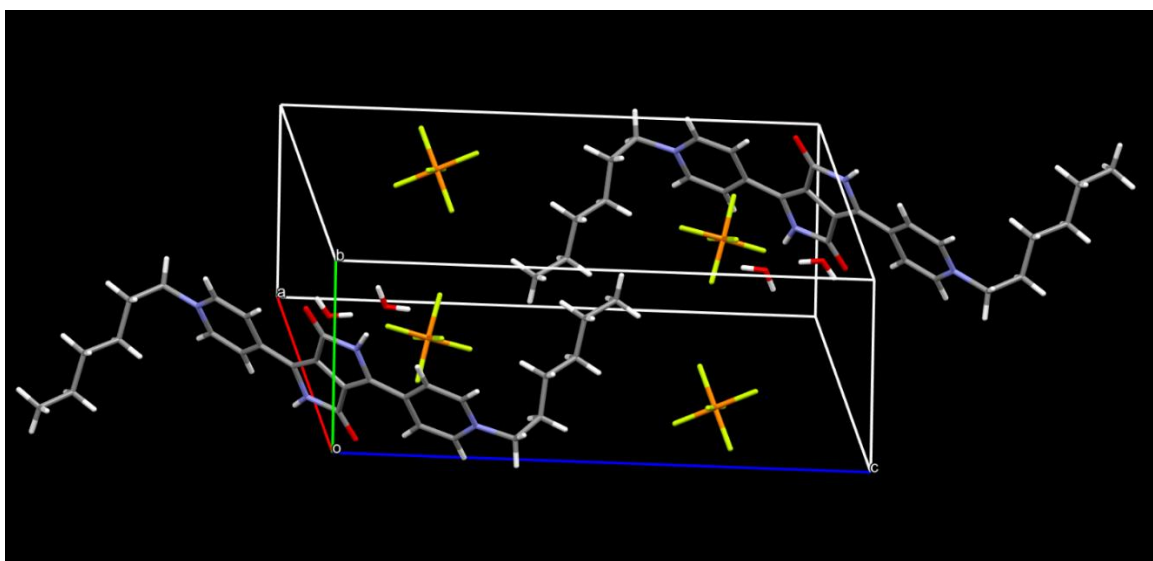


**Figure S38** A view of the crystal packing of 4-2.2PF<sub>6</sub>.

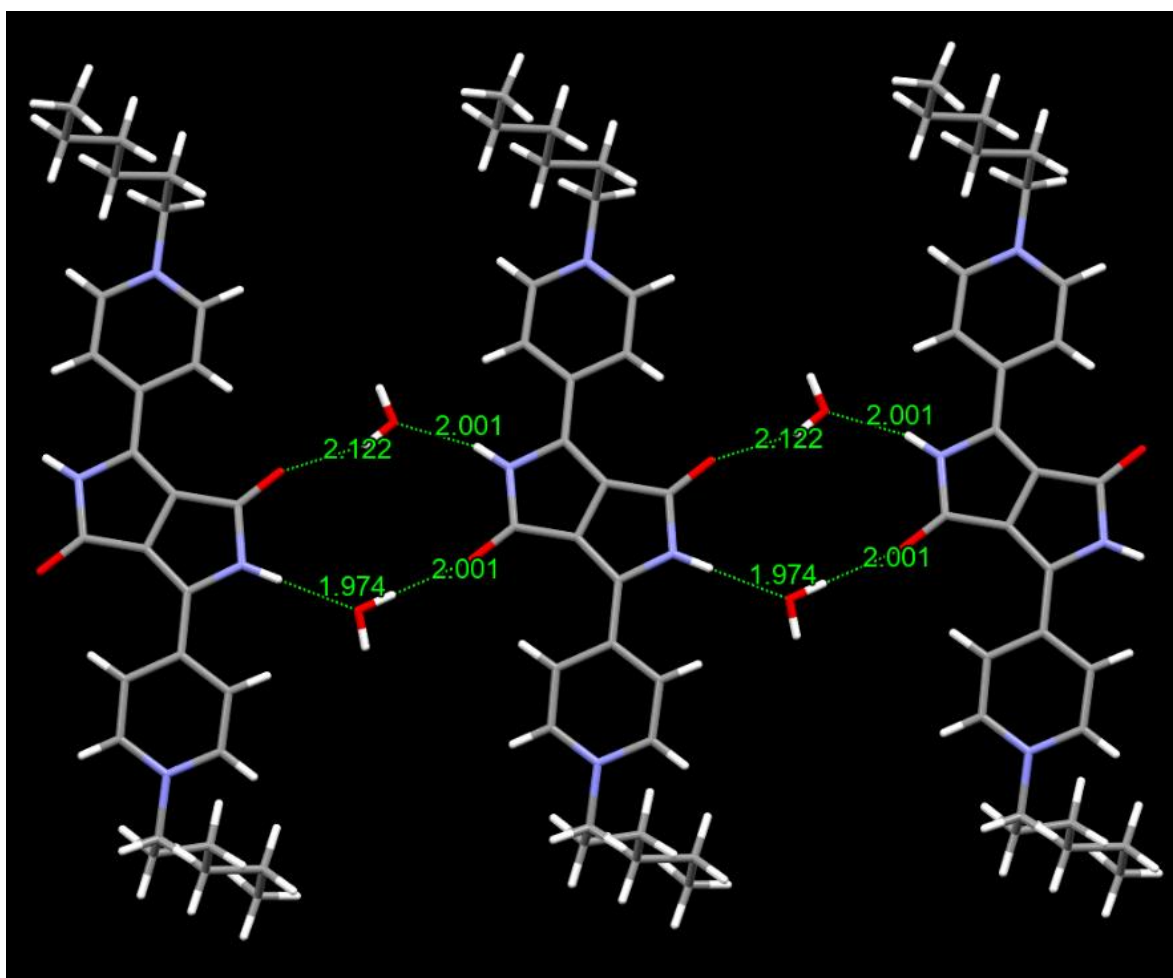


**Figure S39** A view of the crystal structure of 4-2.2PF<sub>6</sub> showing hydrogen bonding of a molecule to four water molecules. Counter anions were omitted for clarity.

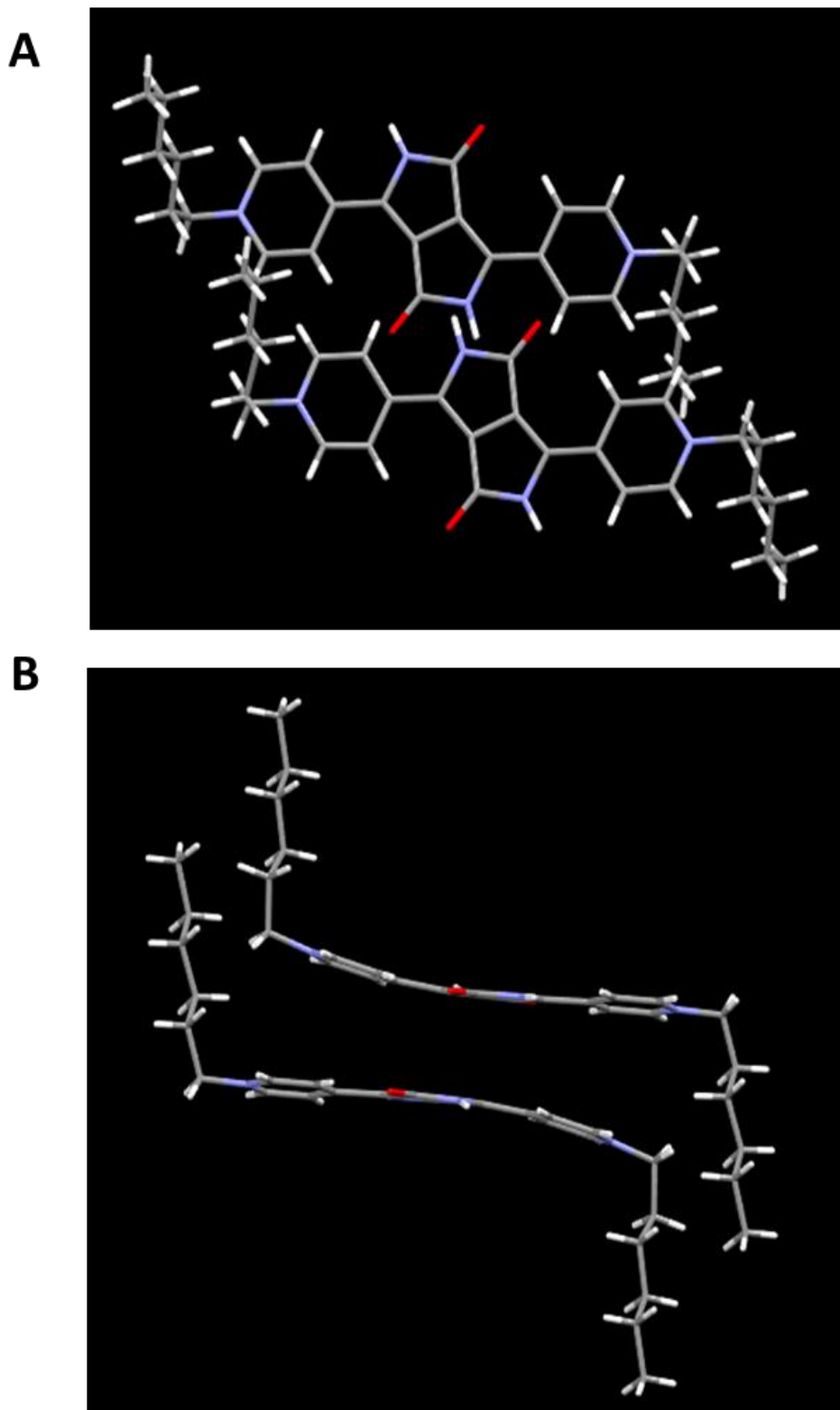


**Figure S40** A view of the crystal structure of 4-2.2PF<sub>6</sub> showing non-overlapping parallel arrangement. **A** top view, **B** lateral view, counter anions omitted for clarity.

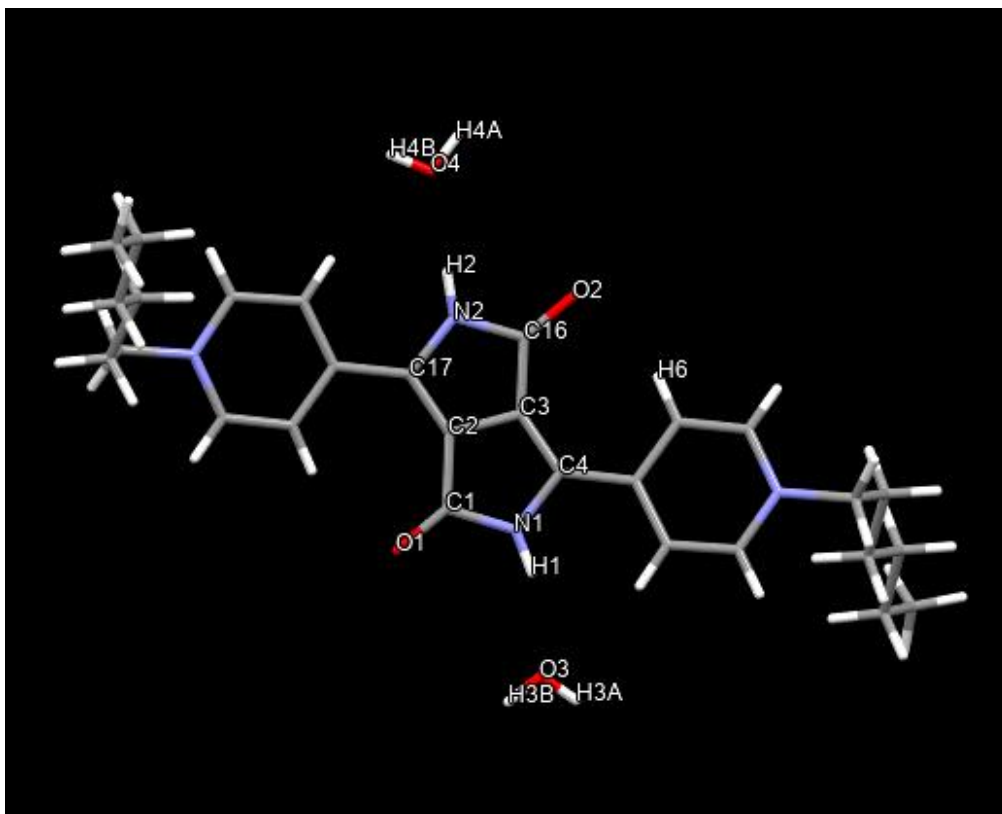


**Figure S41** A view of the crystal structure of 4-2.2PF<sub>6</sub> with labels on the atoms involved in hydrogen bond.

**Table S5.** Selected hydrogen-bond parameters of 4-2.2PF<sub>6</sub>.

<i>D</i> —H··· <i>A</i>	<i>D</i> —H (Å)	H··· <i>A</i> (Å)	<i>D</i> ··· <i>A</i> (Å)	<i>D</i> —H··· <i>A</i> (°)
N1—H1···O3	0.88 (2)	2.00 (3)	2.853 (6)	164 (7)
N2—H2···O4	0.88 (2)	1.98 (2)	2.858 (6)	175 (7)
O3—H3B···O2 <sup>i</sup>	0.79 (7)	2.12 (8)	2.871 (5)	158 (7)
O4—H4A···O1 <sup>ii</sup>	0.85 (2)	2.00 (2)	2.839 (5)	174 (7)
O4—H4B···F2 <sup>iii</sup>	0.84 (2)	2.09 (4)	2.866 (7)	152 (7)

Symmetry code(s): (i) *x*, *y*-1, *z*; (ii) *x*, *y*+1, *z*; (iii) -*x*, -*y*+1, -*z*+2.

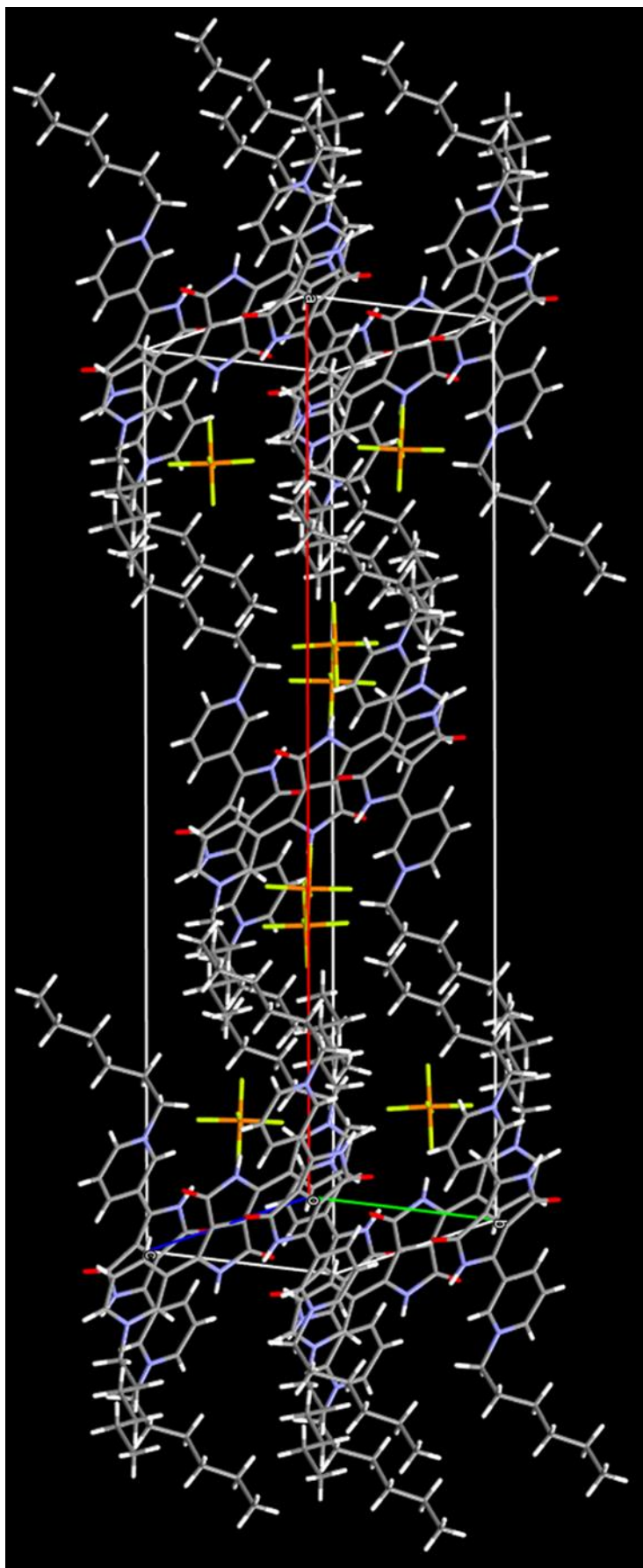


**Figure S42** A view of the crystal packing of 3-2.2PF<sub>6</sub>.

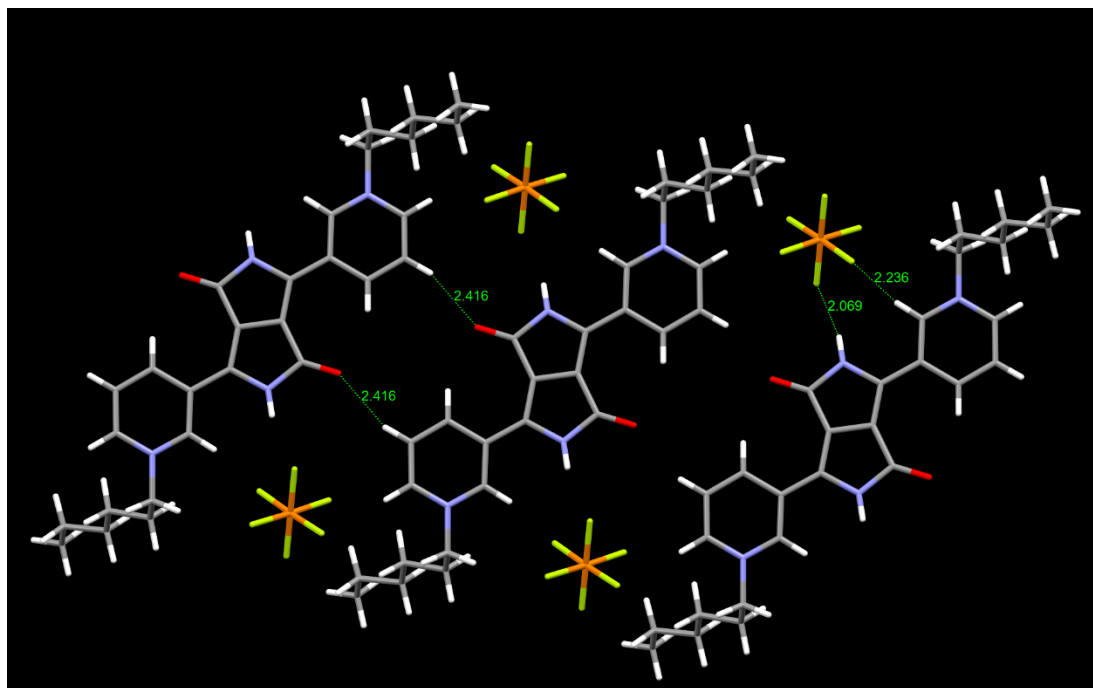


**Figure S43** A view of the crystal structure of 3-2.2PF<sub>6</sub> showing hydrogen bonding between the oxygen of the carbonyl and the hydrogen of the pyridinium ring, and hydrogen bond between the NH moieties and the counter anions.

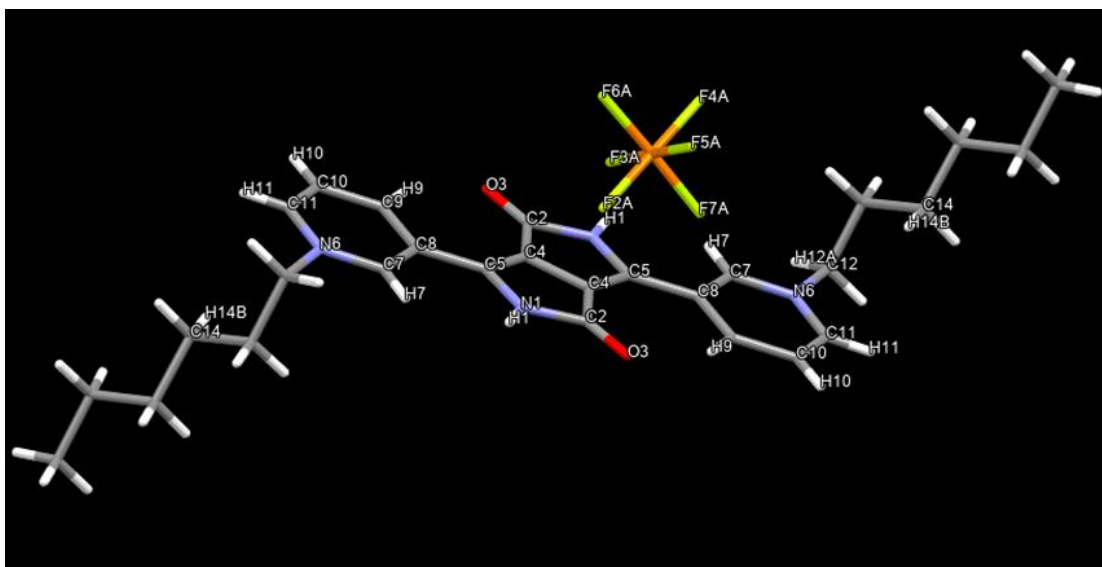
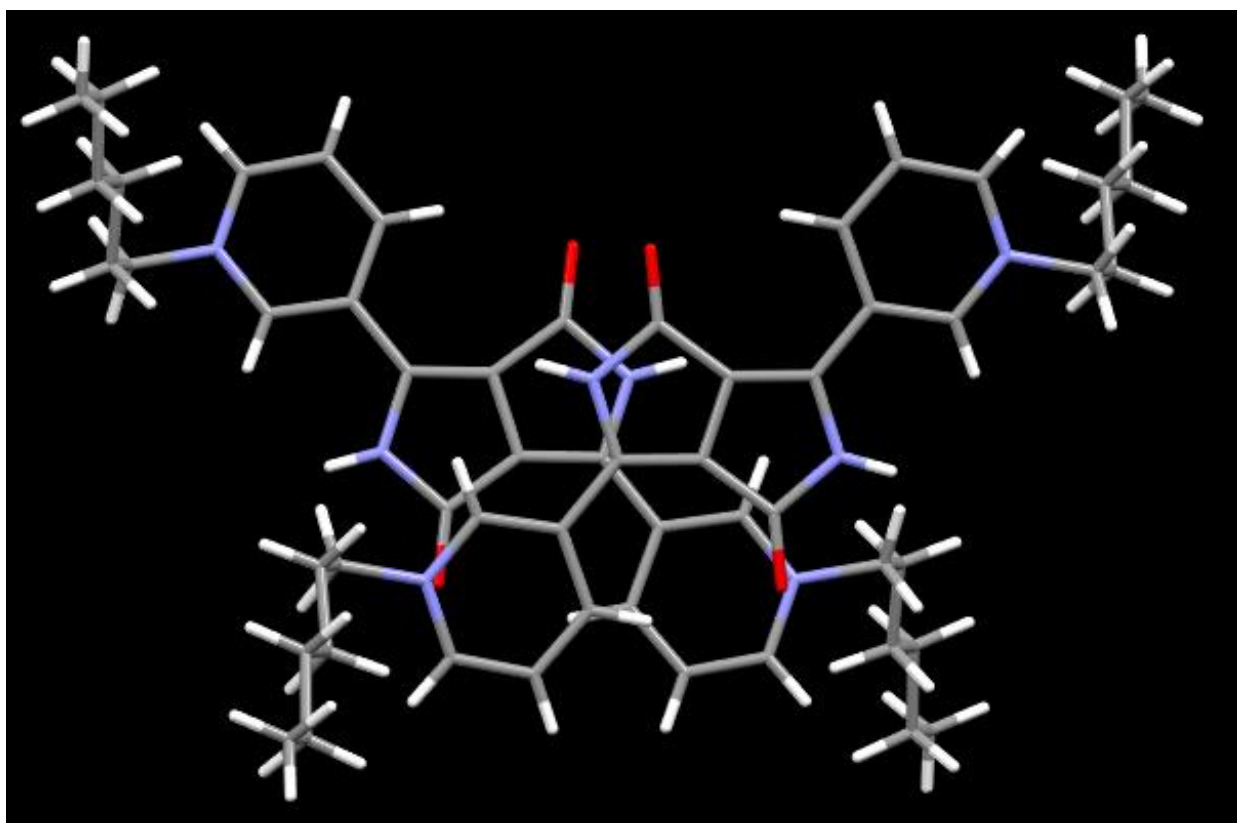


**Figure S44** A view of the crystal structure of 3-2.2PF<sub>6</sub> with labels on the atoms involved in hydrogen bond.

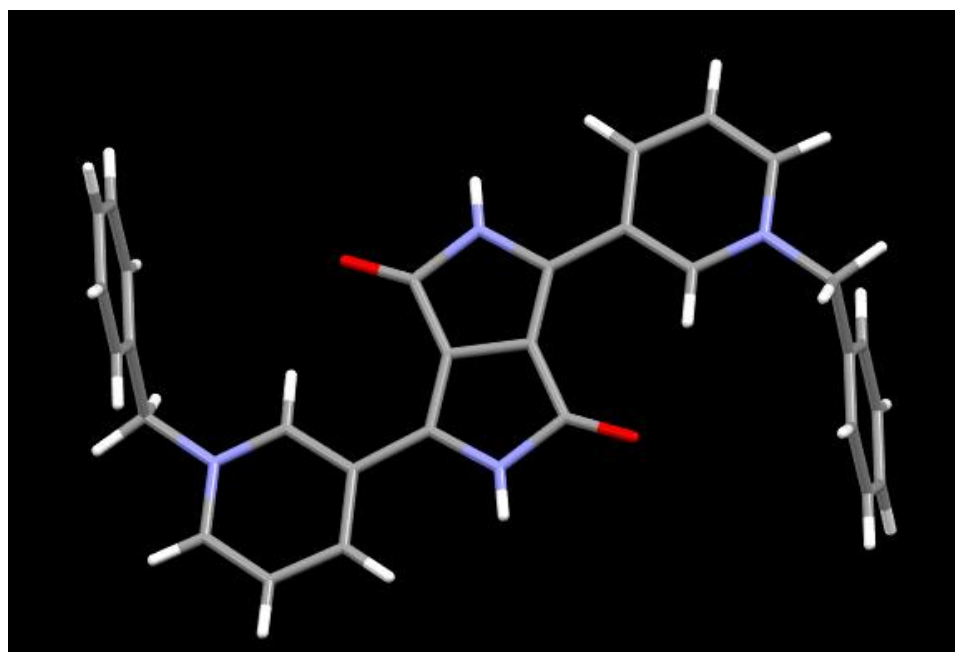
**Table S6.** Selected hydrogen-bond parameters of 3-2.2PF<sub>6</sub>.

<i>D</i> —H... <i>A</i>	<i>D</i> —H (Å)	H... <i>A</i> (Å)	<i>D</i> ... <i>A</i> (Å)	<i>D</i> —H... <i>A</i> (°)
N1—H1...F2A	0.838 (14)	2.069 (15)	2.8599 (16)	157.3 (18)
C7—H7...F5A	0.95	2.24	3.1120 (18)	152.8
C9—H9...O3 <sup>i</sup>	0.95	2.28	3.1669 (19)	155.1
C10—H10...O3 <sup>ii</sup>	0.95	2.42	3.2937 (19)	153.5
C11—H11...F6A <sup>ii</sup>	0.95	2.40	3.0581 (19)	125.7
C12— H12B...F6A <sup>iii</sup>	0.99	2.38	3.162 (2)	135.4
C14— H14B...F6A <sup>ii</sup>	0.99	2.63	3.2382 (19)	120.0

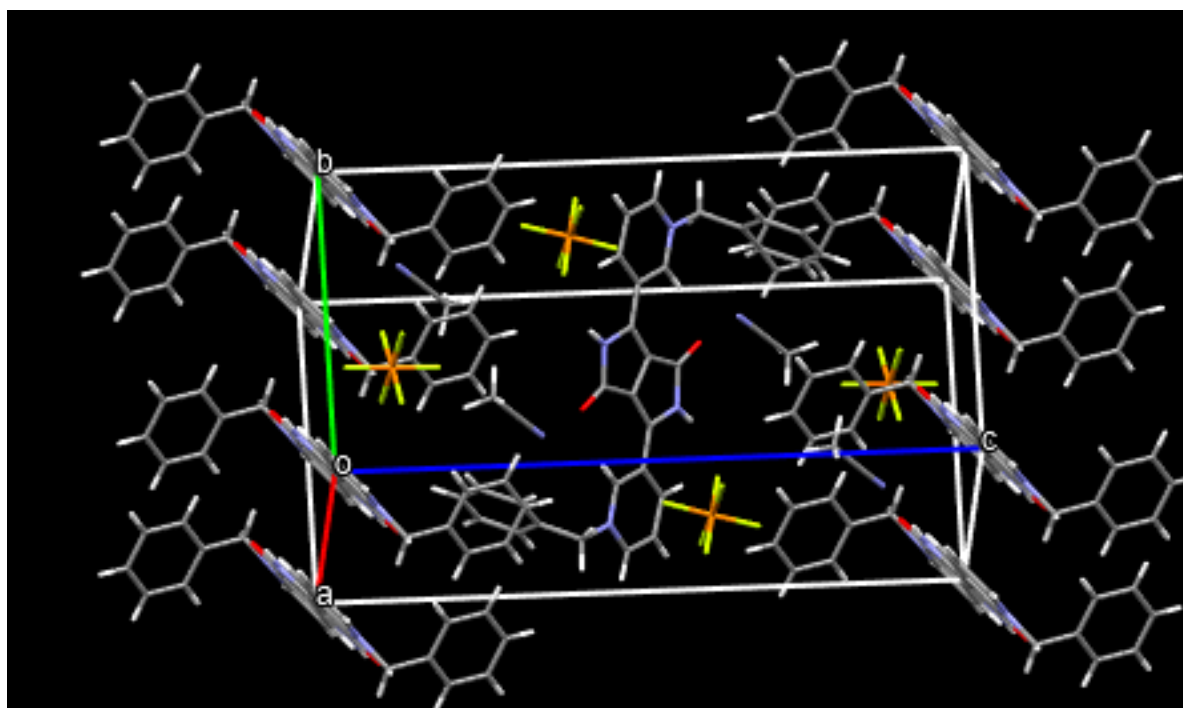
Symmetry code(s): (i)  $-x+1, -y+1, -z+1$ ; (ii)  $x, y-1, z$ ; (iii)  $x, -y+1, z+1/2$ .



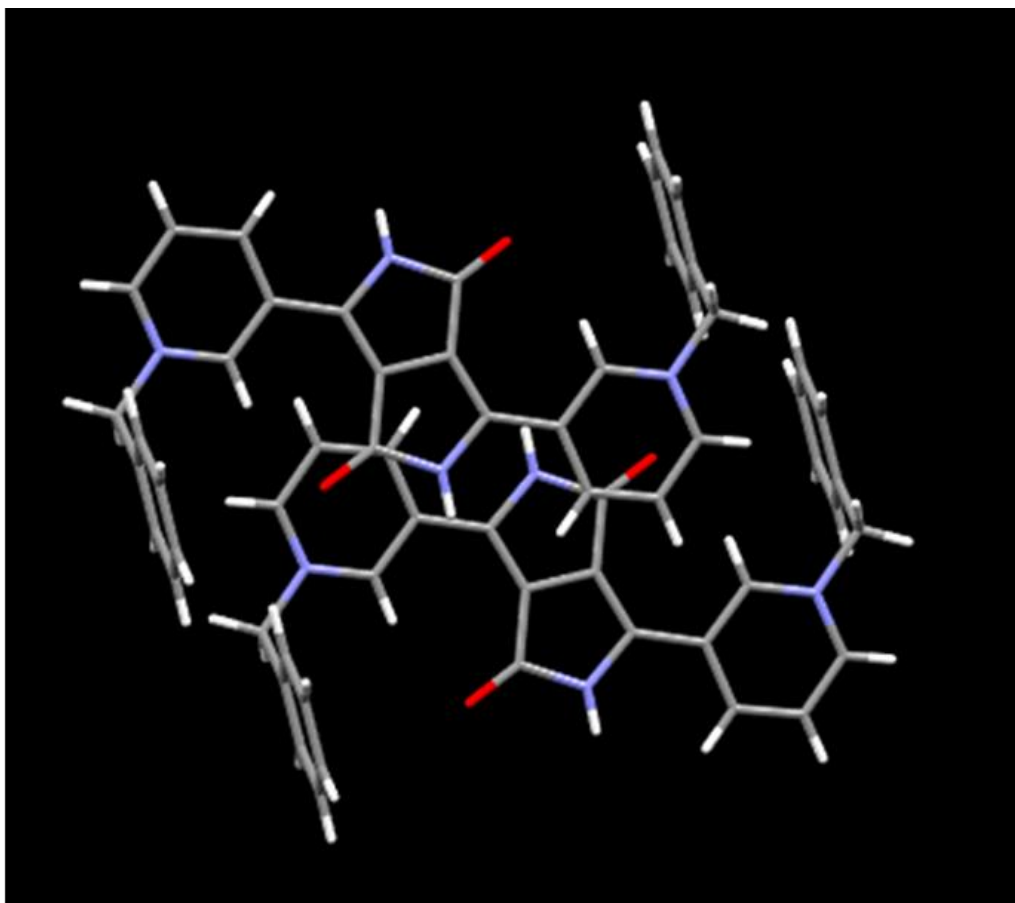
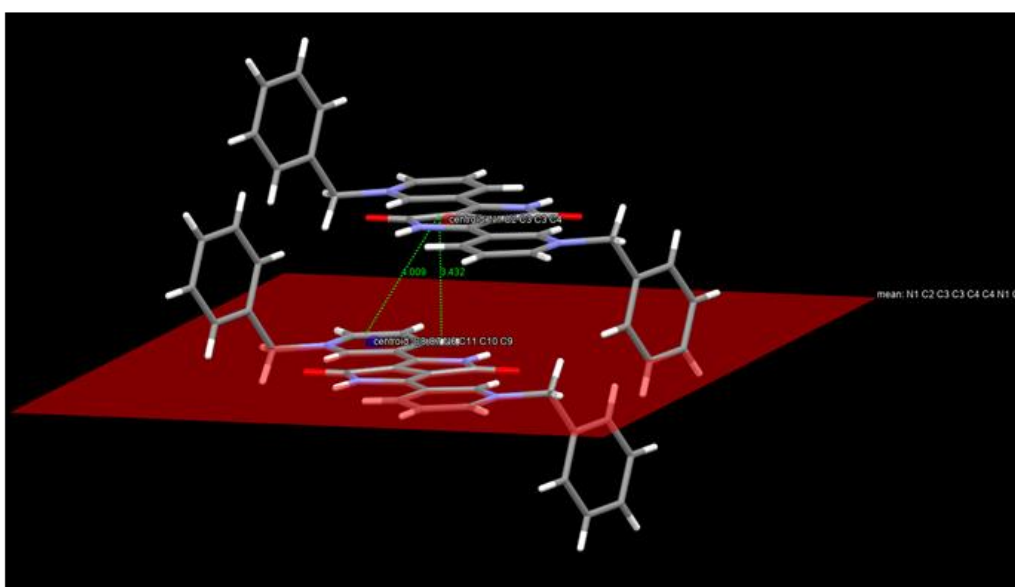
**Figure S45** A view of the crystal structure of 3-2.2PF<sub>6</sub> showing the minimal overlap of the aromatic systems. Counter anions are omitted for clarity.



**Figure S46:** Crystal structure of 3-3.2PF<sub>6</sub> showing a single molecule. Counter anions are omitted for clarity.



**Figure S47** A view of the crystal packing of 3-3.2PF<sub>6</sub>.

**A****B**

**Figure S48** Views of the crystal structure of 3-3.2PF<sub>6</sub> showing the minimal overlap of the aromatic systems, (A) top view, (B) showing distance between lactam centroid and aryl centroid, and lactam centroid and aryl plane. Counter anions are omitted for clarity.

**Table S7.** GI<sub>50</sub> (Concentration which inhibits cell proliferation by 50%) and LC<sub>50</sub> (Concentration which kills 50% cells from time of treatment) values for Paraquat, 4-2.2PF<sub>6</sub> and 4-3.2PF<sub>6</sub>

Cell line	GI <sub>50</sub> (μM)		LC <sub>50</sub> (μM)	
	A549	MRC-5	A549	MRC-5
Paraquat	4.90; 4.47	5.60; 5.50	>100; 75.1	84.2; 80.9
4-2.2PF <sub>6</sub>	>100; >100	>100; >100	>100; >100	>100; >100
4-3.2PF <sub>6</sub>	>100; >100	>100; >100	>100; >100	>100; >100

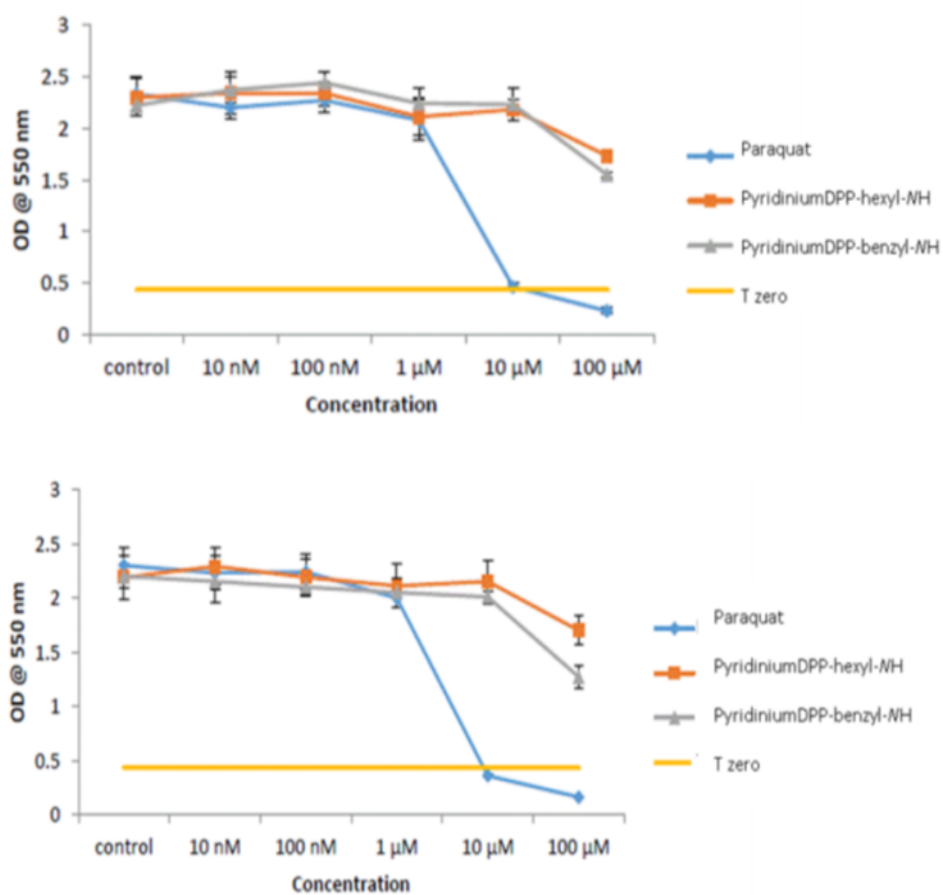


**Figure S49** MTT assay for A549 carcinoma cell after addition of compound showing optical density at 550 nm vs. concentration.

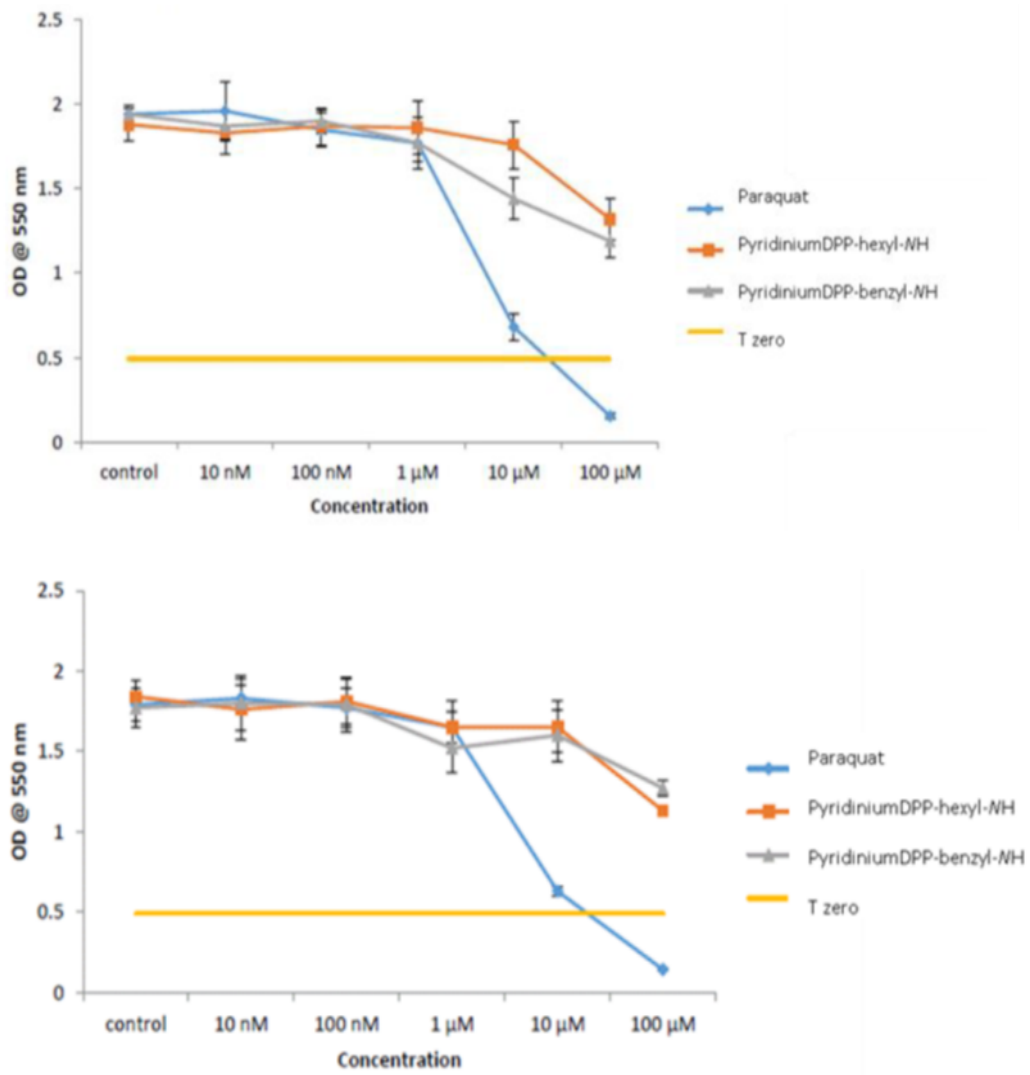


**Figure S50** MTT assay for MRC-5 Fibroblast growth after addition of compound showing optical density at 550 nm vs. concentration.